PART I. KINETICS OF COARSENING OF THE GAMMA-PRIME PRECIPITATE IN NICKEL-SILICON ALLOYS

PART II. RATE OF CRYSTALLIZATION OF AN AMORPHOUS Fe-P-C ALLOY

Thesis by

Prabhat Kumar Rastogi

In Partial Fulfillment of the Requirements

For the Degree of

Doctor of Philosophy

California Institute of Technology

Pasadena, California

1970

(Submitted March 9, 1970)

To my Wife and Parents

ACKNOWLEDGEMENTS

The author wishes to express his deepest gratitude to Professors Pol E. Duwez and A. J. Ardell, now at U. C. L. A., for their valuable suggestions and constant encouragement throughout this work. He would also like to thank Drs. C. C. Tsuei, R. E. Villagrana and R. Hasegawa for their helpful discussions. Technical assistance provided by F. G. Youngkin, J. E. Brown, J. A. Wysocki and C. Geremia during various phases of the work is greatly appreciated.

He is grateful to Mrs. V. Conner and Mrs. Elizabeth G. Wolar for their cooperation in typing the manuscript and to his wife Sanju for her patience and encouragements during the present work.

Financial aid was gratefully received from the Atomic Energy Commission.

Part I - ABSTRACT

The coarsening kinetics of $Ni_3Si(\gamma')$ precipitate in a binary Ni-Si alloy containing 6.5 wt. % silicon was studied by magnetic techniques and transmission electronmicroscopy. A calibration curve was established to determine the concentration of silicon in the matrix. The variation of the Si content of the Ni-rich matrix as a function of time follows Lifshitz and Wagner theory for diffusion controlled coarsening phenomena. The estimated values of equilibrium solubility of silicon in the matrix represent the true coherent equilibrium solubilities.

The experimental particle-size distributions and average particle size were determined from dark field electron micrographs. The average particle size varies linearly with $t^{-\frac{1}{3}}$ as suggested by Lifshitz and Wagner. The experimental distributions of particle sizes differ slightly from the theoretical curve at the early stages of aging, but the agreement is satisfactory at the later stages. The values of diffusion coefficient of silicon, interfacial free energy and activation energy were calculated from the results of coarsening kinetics. The experimental value of effective diffusion coefficient is in satisfactory agreement with the value predicted by the application of irreversible thermodynamics to the process of volume constrained growth of coherent precipitate during coarsening. The coherent γ' particles in Ni-Si alloy unlike those in Ni-Al and Ni-Ti seem to lose coherency at high temperature. A mechanism for the formation of semi-coherent precipitate is suggested.

Part II - ABSTRACT

An alloy containing iron, phosphorous and carbon in the atomic concentrations corresponding to Fe_{75}-P_{15}-C_{10} can be obtained in the amorphous state by rapid quenching from the liquid state. The transformation of this alloy from the amorphous to the equilibrium crystalline state has been studied by thermal analysis, x-ray and electron diffraction, electronmicroscopy and electrical resistivity. At rates of heating above about 320°C/min, the alloy transforms very rapidly into a microcrystalline structure with an average crystal size of about 300 Å. At slightly lower rates (about 100°C/min) it is possible to stop the massive crystallization and microcrystalline clusters of metastable phases imbedded in an amorphous matrix are present. At a relatively low rate of heating of 1°C/min, crystallization starts around 375°C, but has a sudden increase in the range of 420 to 440 °C. This increase in crystallinity is reflected in the electrical resistivity which also shows a sharp drop within the same temperature range. Before this massive crystallization takes place, the electrical resistivity increases slowly with temperature. This behavior has been observed previously in a number of amorphous alloys. In the amorphous FePC alloy, this increase in resistivity is not a reversible phenomenon, and the results of the present investigations suggest that it is due to additional scattering of the conduction electrons by very small clusters of crystalline phases, about 50Å in size.

TABLE OF CONTENTS

TABLE OF CONTENTS (Cont'd)

PART I. KINETICS OF COARSENING OF THE GAMMA-PRIME PRECIPITATE IN NICKEL-SILICON ALLOYS

I. I. INTRODUCTION

Nickel-base alloys constitute an important class of materials for high strength applications at elevated temperatures. Although most of the practical alloys contain more than one alloying element, the binary alloys Ni-Al, Ni-Ti and Ni-Si are of fundamental interest. These solid-solution alloys can be hardened by precipitation of the so-called gamma prime phase. The strength properties of these alloys are mainly due to the size, the shape, the distribution of the particles, and their interaction with dislocations. The γ' phase has an ordered face-centered cubic lattice. During the precipitation process nuclei are formed and grow in size until the surrounding matrix reaches the equilibrium concentration at the aging temperature.

It has been found that after a certain particle size (of the order of 50 A) has been reached, the growth of the precipitate can be described as an 'Oswald ripening', and the driving force for growth has its origin in the interfacial energy between matrix and precipitate. Lifshitz and Slyozov[1] and Wagner[2] independently proposed similar theories for diffusion controlled coarsening. Although these theories are strictly valid for coarsening of spherical particles in a fluid matrix, Li and Oriani[3] have shown that the same theoretical approach can be applied to particle coarsening in a solid matrix. The Lifshitz-Wagner theory has been successful in explaining the coarsening of precipitates in Ni-Al and Ni-Ti alloys, but some discrepancies still exist between theory and experiments. Ardell[4] for example, has shown that the experimentally observed particle size distributions in these two systems do not exactly follow the theoretical predictions,

and the discrepancy is probably associated with the misfit between the lattice of the matrix and that of the precipitate. From that point of view, the Ni-Si alloys chosen for the present investigation are of interest because in this system the lattice misfit is relatively low. In addition it was found that in this system, contrary to what was observed in Ni-Al and Ni-Ti, the precipitate loses coherency at high temperature.

I. II. EXPERIMENTAL PROCEDURE

A. Specimen preparation

Both Ni and Si used for preparing the alloys had a purity greater than 99.9999%. The alloys were melted either in an alumina crucible under argon atmosphere or by induction on a water cooled silver boat. All alloys had a nominal composition of 6.5 wt. %Si, and since no measurable weight losses occurred after melting it was assumed that the nominal composition was the actual one. The alloys melted in an alumina crucible were cast into cylindrical rods by sucking the melt into a fused silica tube 2 mm in diameter. These rods were then cold rolled into bars with a square cross section of approximately 1 mm^2. These specimens were used for magnetic measurements. The alloys prepared by silver boat melting were swaged into bars about 2.5 mm in diameter. After solution heat treatment, these bars were rolled into sheets down to a final thickness of about 100μ. These specimens were used for electronmicroscopy.

The etching of the alloy foils was performed first by the jet technique and then by the window technique. The jet etching was made in a solution containing 20% volume hydrochloric acid, 15% perchloric acid, 20% nitric acid and 45% water. The potential was between 80 and 90 V dc. Final polishing was made in a solution containing 87% volume methanol and 13% hydrochloric acid maintained at -50°C in a dry ice-acetone mixture, with a voltage of 10 to 15 V dc. The formation of a hole in the specimen was detected by an optical microscope and the areas of the specimen around that hole were thin enough for transmission microscopy.

B. Magnetic Measurements

Since the change in the Curie temperature was used for studying the progress of precipitation, it was necessary to establish a 'calibration curve' of Curie temperature vs. Si content for the equilibrium alloys containing increasing amounts of Si. The specimen, in the form of a rod was placed inside an induction coil, and the transition from ferromagnetic to paramagnetic was detected by the unbalance of a Wheatstone bridge. A schematic diagram of the experimental apparatus is shown in Fig. 1. An especially designed furnace was placed around the specimen for high temperature measurements, and a liquid nitrogen bath was used for measurement below room temperature. The rate of heating above liquid nitrogen temperature was slow enough to detect the transition. A copper-constantan thermocouple (0.0068" in diameter) was spot welded to the specimen. The calibration curve showing the Curie temperature vs. Si content is shown in Fig. 2. As shown in Fig. 2 the relationship between Curie temperature and Si content is linear and can be represented by the empirical equation

$$W_{si} = \frac{420.66 - \theta_c}{93.33} \qquad (1)$$

in which θ_c is the Curie temperature expressed in °C and W_{si} is the Si content in weight percent.

C. Aging Experiments

The specimens were first solution treated for 2 hours at 1100°C and quenched in water. Aging was carried out in an atmosphere of titanium gettered argon at 775, 725, 682, 652 and 625°C, in a furnace whose temperature was controlled within ± 1°C. After a given aging

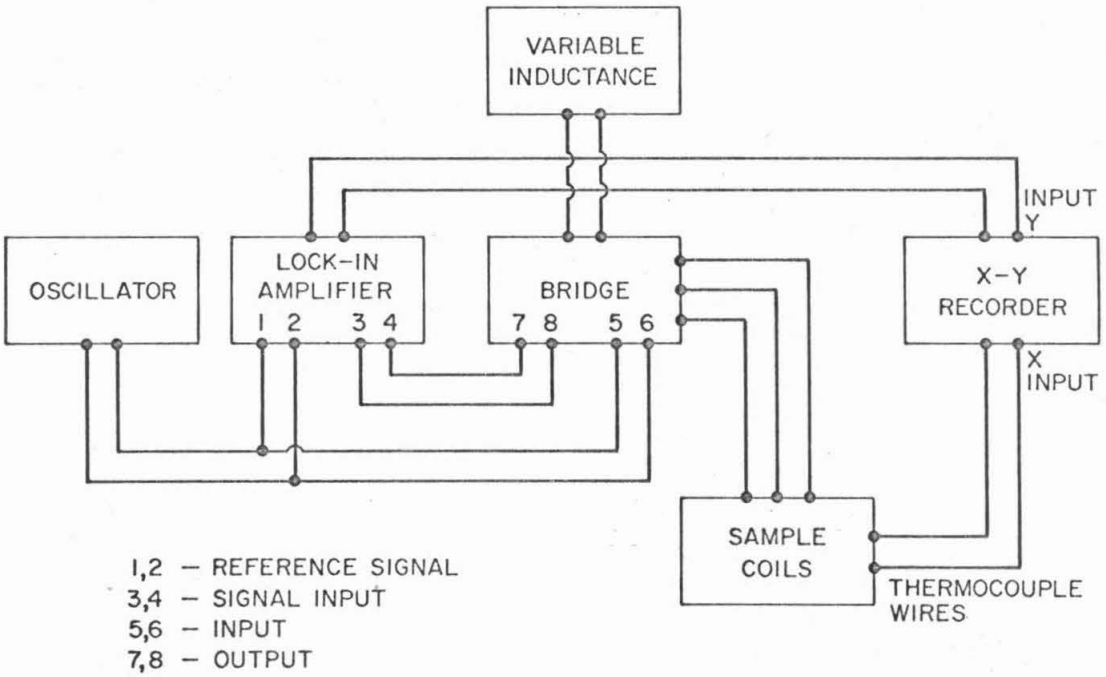

Fig. 1. Schematic circuit diagram for measuring the Curie temperature.

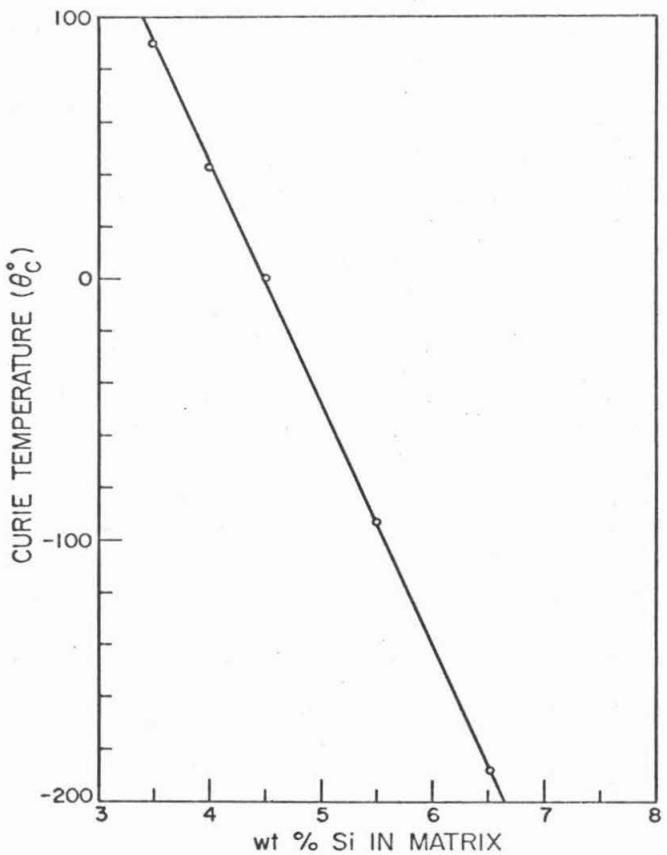

Fig. 2. Calibration curve of ferromagnetic Curie temperature Θc vs. wt. % Si in the Ni matrix.

time, the specimen was quenched in water, its Curie temperature was measured, and the aging treatment was continued until equilibrium was achieved. A typical curve of magnetization vs. thermocouple emf is shown in Fig. 3. The Curie temperature was taken at the intersection of a straight line drawn through the steepest portion of the curve and the extrapolated paramagnetic portion of the curve.

D. Estimated Uncertainties in Measurements

The Curie temperature measurements were sensitive enough to detect changes in the silicon concentration in the matrix of approximately 0.002 wt. %. On the other hand the absolute values of the silicon concentration depend primarily on the accuracy of the calibration curve. In order to check the results of the magnetic measurements the following experiments were performed.

A sheet specimen of the Ni-Si alloy was aged for 48 hours at 700°C in order to produce a homogeneous dispersion of the Ni_3Si (γ') precipitate. The aging treatment was then continued for $1\frac{1}{2}$ hours at increasing temperatures approaching the equilibrium solubility temperature predicted by the magnetic measurements, namely 835°C (Fig. 4). Electronmicroscopy examination revealed that the precipitate was present at 835°C but was not detected at 855°C. In the range of 835°C to 855°C, the change in silicon concentration is of the order of ± 0.01%, which is negligible.

E. Electronmicroscopy

All specimens were examined with both bright and dark field in a Siemens Elmiskop I electronmicroscope with a voltage of 100 kV. Dark field micrographs were obtained by using superlattice reflections

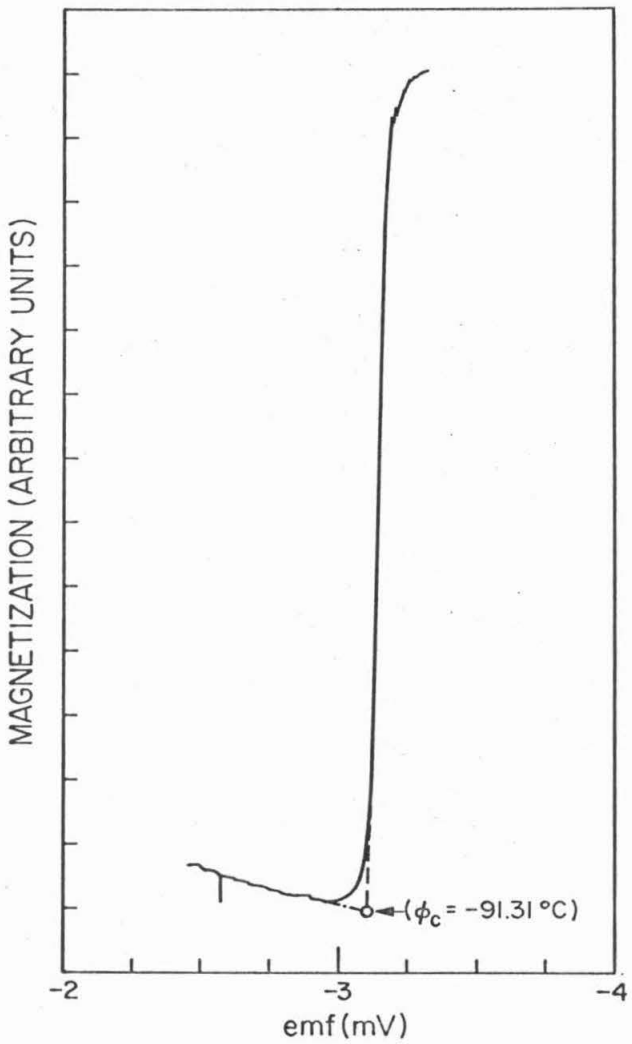

Fig. 3. Typical recording of specimen magnetisation vs. thermocouple emf for 6.5 wt% Si alloy aged 4 h. at 652°C.

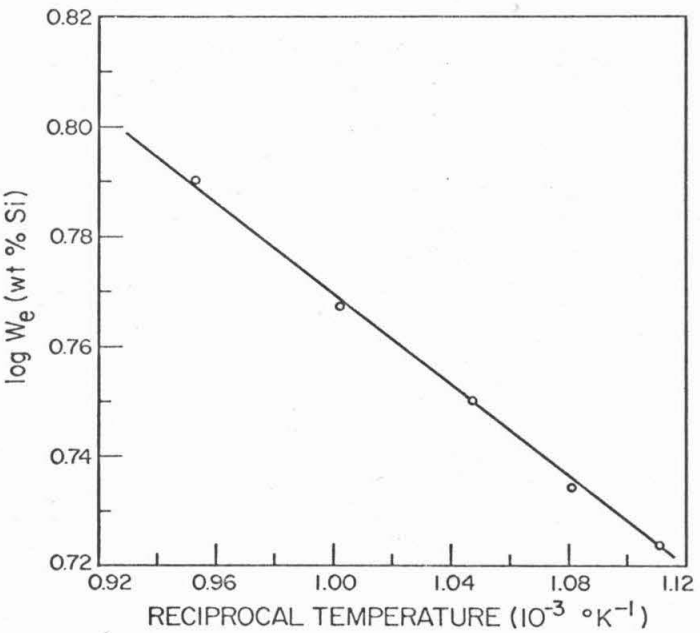

Fig. 4. Arrhenius plots of the equilibrium solubilities of γ' precipitate in Ni-Si alloys.

from the ordered precipitates. Standard gun-tilting procedures were used to avoid excessive aberration. Dark field technique was useful because the particle shapes and sizes were always well defined. This was not the case with bright field images because of the coherency strain contrast, especially in the case of very small particles. Dark field micrographs were taken from foils in the (110) orientation and particle sizes were measured along the (100) direction in the plane of the foil. Foils having the (100) orientation were never found. The mean particle edge $\bar{a}$ was deduced from the arithmetic mean of 50 measurements. The precipitate particles were approximately spherical in shape for very short aging times and in that case measurements could be made in any arbitrary direction. The magnifications of the micrographs were corrected for small changes resulting from different focusing conditions from sample to sample. The uncertainty in particle size measurements is estimated to be about $\pm 5\%$

I. III. THEORETICAL CONSIDERATIONS

A. Growth of the average particle

It is known [1, 2] that coarsening processes occur by the diffusion controlled transfer of solute in the matrix. The driving force for particle growth is mostly due to the reduction of the total amount of the interfacial energy of the particles. For the ideal case of spherical particles coarsening in a fluid matrix, Lifshitz and Slyozov[1] and Wagner[2] have developed the following equations for the growth of the average particle as a function of time.

$$\overline{r}^3 - \overline{r}_o^3 = 2\gamma D C_e V_m^2 t/\rho_c^2 RT \qquad (2)$$

where $\overline{r}_o$ = mean particle radius at the start of Oswald ripening

$\overline{r}$ = average particle radius at time t

γ = interfacial free-energy of the particle-matrix interface

C_e = concentration of the solute in the matrix in equilibrium with a particle of infinite radius

V_m = molar volume of the precipitate

T = temperature in °K

R = Gas constant

ρ_c = 3/2 (related to theoretical distribution of particle sizes)

B. Theoretical distribution of particle sizes

The quasi-steady state distribution (2) of particle sizes f(r, t) is related to any arbitrary initial distribution f(r, o) by the following equation:

$$f(r, t) = f'(t)\, \rho^2 h(\rho) \qquad (3)$$

Where f(t) is function of time only, $\rho = \frac{r}{\bar{r}}$ and $h(\rho)$ is given by

$$h(\rho) = \left[\frac{3}{3+\rho}\right]^{7/3} \left[\frac{3/2}{3/2-\rho}\right]^{1/3} \exp\left[\frac{-\rho}{3/2-\rho}\right] \tag{4}$$

Equation (4) is only valid for $\rho < \rho_c = 3/2$. For $\rho > \rho_c$. $h(\rho) = 0$

The distribution curve given by Eq. (4) has the following properties: (a) at $\rho = 3/2$ the curve drops sharply; (b) $h(\rho)$ has a maximum at $\rho = 1.135$; (c) $\int_0^\infty \rho^2 h(\rho) d\rho = 9/4$. This stationary distribution is derived from a narrow Gaussian distribution which is considered to be at the start of growth. The Gaussian distribution in this investigation corresponds to the statistical concentration fluctuations present in the solid solution before the beginning of the aging. Spherical particle shape and homogeneous site distribution should be assumed for the application of the theory. The theory is only valid for small volume fractions of the particles.

C. Average concentration of solute in the matrix

The average concentration of the solute in the matrix is related to the average particle radius $\bar{r}$ by Gibbs-Thomson equation

$$C - C_e = \frac{2\gamma C_e V_m}{\bar{r} R T} \tag{5}$$

where C is the concentration of the solute in the matrix at any time t. Let us denote $C - C_e = \Delta$ and using Eq. (2) and Eq. (5) we get

$$\frac{1}{\Delta^3} - \frac{1}{\Delta_o^3} = \eta t \tag{6}$$

where $$\eta = \frac{D(RT)^2}{9\gamma^2 C_e^2 V_m} \tag{7}$$

and $$\Delta_o = C_o - C_e$$

At longer aging times $1/\Delta_o^3$ is negligible compared to $1/\Delta^3$ due to the asymptotic behavior of the Eq. (6). Then Eq. (5) can be rewritten as

$$\Delta = C - C_e = (\eta t)^{-1/3} \tag{8}$$

The true behaviour of the general expression (6) can be checked at very short aging time. In the present case however, the investigation has been carried out only for long aging times.

D. Time dependence of the volume fraction of precipitate

It is generally assumed that the volume fraction of precipitate remains constant during coarsening. But there is a small change in volume fraction of precipitate compared with that which occurs during the early stages of precipitation. It is clear from the lever rule that an increase in volume fraction of precipitate is associated with a decrease in solute concentration. If Φ denotes the volume fraction of precipitate, W_i the total wt. fraction of solute in the alloy and $W_{\gamma'}$ the wt. fraction of solute in the γ' phase we get

$$\Phi = \frac{W_i - W(t)}{W_{\gamma'} - W(t)} \tag{9}$$

Here the densities of the γ' phase and that of the matrix have been assumed to be the same. Using Eq. (8) for wt. fraction in Eq. (9) we get

$$\Phi = \frac{W_i - W_e - (\eta t)^{-1/3}}{W_{\gamma'} - W_e - (\eta t)^{-1/3}} \tag{10}$$

Equation (10) is only valid for long aging times. By expanding the denominator of Eq. (10) and ignoring all terms of higher order than $(\eta t)^{-1/3}$ we get

$$\Phi = \Phi_e - (\eta^* t)^{-1/3} \tag{11}$$

where

$$\Phi_e = \frac{W_i - W_e}{W_{\gamma'} - W_e} \qquad \text{and}$$

$$\eta^* = \left[\frac{W_{\gamma'} - W_e}{1 - \Phi_e}\right]\eta$$

Physically, Φ_e denotes the equilibrium volume fraction of γ' precipitate and W_e is the equilibrium wt. fraction of the solute in the matrix. It is seen from Eq. (11) that there is a linear relationship between Φ and $t^{-1/3}$ and therefore, the constancy of the volume fraction of precipitate is not a good assumption.

I. IV. EXPERIMENTAL RESULTS

A. Equilibrium Solubility

The silicon content in the matrix during aging was determined by magnetic measurements and using the calibration curve shown in Fig. 2. The experimental values of the weight fraction of silicon in the matrix are plotted against time$^{-1/3}$ and are shown in Fig. 5. These results are in good agreement with Eq. (8). The values of equilibrium solubility W_e of silicon are obtained by extrapolating the curve to infinite time. The slope of these curves yields the values of the rate constant η. The values of W_e and η are given in Table I. The equilibrium solubility concentrations are about 5% larger than those reported by Hansen.[5] The value of the activation energy Q for diffusion of solute is obtained from a plot of $\eta W_e^2/T^2$ against $1/T$. The slope of this straight line (shown in Fig. 6) yields a value $Q = 62.6$ kcal/mole.

The concentration of Si in the matrix in the specimens aged at 775°C shows a marked decrease for aging times above 17 hours. The latter part of the curve shown in Fig. 7 does not fit Eq. (8). The sudden change in the silicon concentration vs. time was not observed in the experiments performed at 625, 682, and 725°C. To understand this peculiar behavior, a sample was aged at 652°C and after 81 hours it was then plastically deformed by rolling, with a 50% reduction in cross-section. Three measurements were taken after various aging times and a sharp decrease in solute concentration was observed. On the other hand no drastic change in concentration was observed for specimens plastically deformed about 25%. Both of these observations seem to indicate that the particles become semicoherent and finally

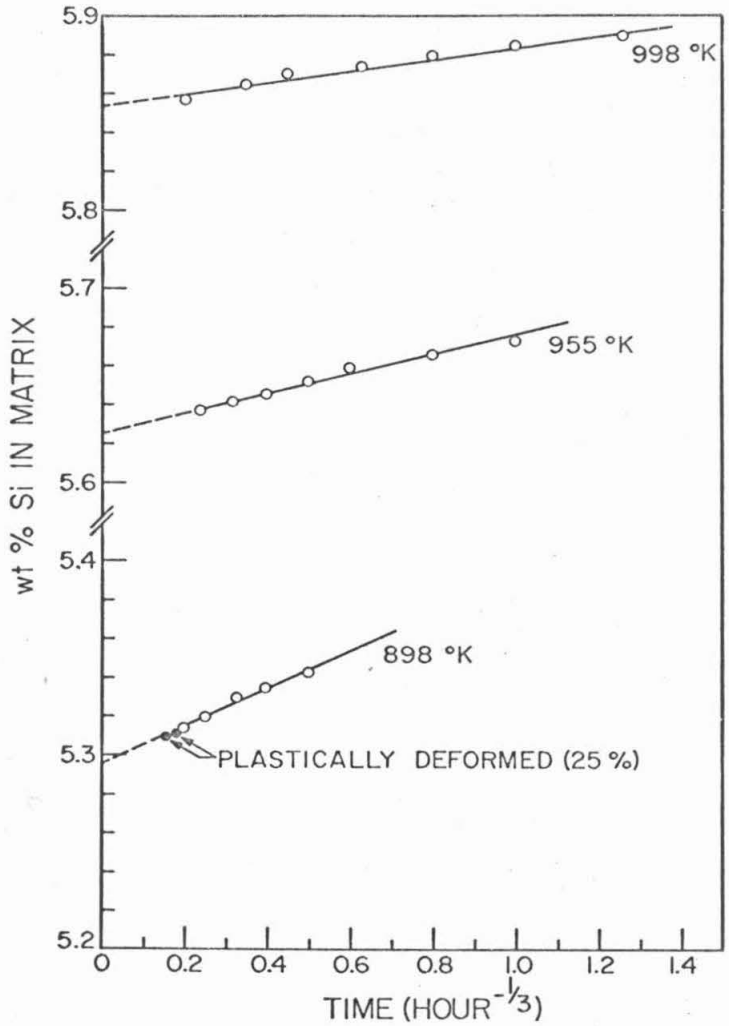

Fig. 5. Plot of wt % Si in the Ni matrix during coarsening of γ' precipitate against $t^{-1/3}$ at different temperatures.

TABLE I

VALUES OF THE COARSENING PARAMETERS FOR γ' PRECIPITATE IN Ni-Si ALLOYS

Aging Temp. T (°C)	Rate Constant η (Sec^{-1})	Equilibrium Solubility W_e (wt. %)
625	2.99×10^{5}	5.296
682	2.28×10^{6}	5.626
725	1.05×10^{7}	5.854

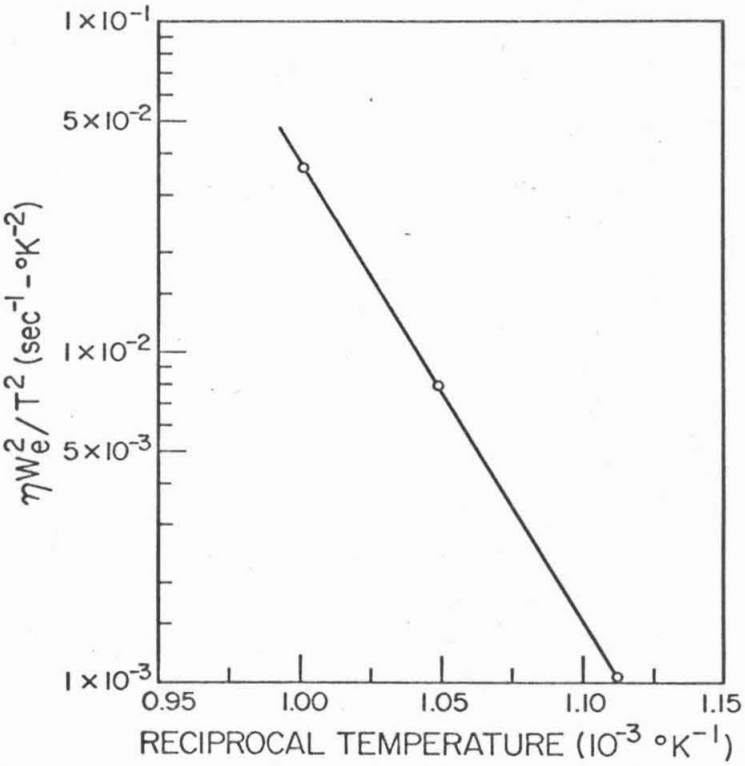

Fig. 6. Arrhenius plot of the rate constants η compensated for the temperature dependent factor W_e^2/T^2 in a Ni-6.5 wt% Si alloy.

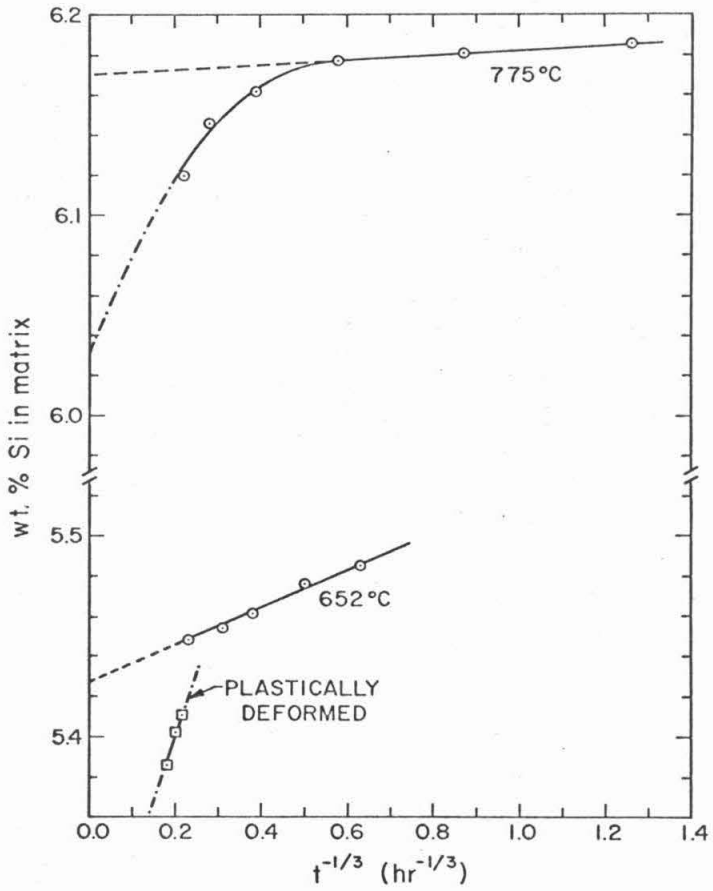

Fig. 7. Sharp decrease in the concentration of Si in the Ni matrix at 775°C and 652°C with 50% deformation.

tend to become truly incoherent with the matrix.

B. Kinetics of particle growth

Specimens were aged at 775°C and particle sizes were determined from dark-field electronmicrographs shown in Figs. 8 to 11. In the early stages of aging the particles were nearly spherical and later on they became cuboidal in shape. The measurements were made along the (100) direction and the average particle size was given by the arithmetic mean of 50 measurements. We know that,

$$\bar{r}^3 - \bar{r}_o^3 = \frac{8 \gamma D C_e V_m^2 t}{9 R T} \qquad (2)$$

For cube shaped particles $r = \bar{a}/2$ where $\bar{a}$ is the average length of the cube edge. Eq. (2) may be rewritten as

$$\bar{a}^3 - \bar{a}_o^3 = \frac{64 \gamma D C_e V_m^2 t}{9 R T} = kt \qquad (12)$$

where

$$k = \frac{64 \gamma D C_e V_m^2 t}{9 R T} \qquad (13)$$

The measured values of $\bar{a}^3$ are plotted against time in Fig. 12 and it obeys Eq. (12). The intercept and slope of the curve yield the values of $\bar{a}_o^3$ and the rate constant k. Using our values of k at 775°C and Hornbogen's values[6] of k at 600°C and 750°C, and taking into account the dependence of concentration on temperature, the value of the activation energy Q for the diffusion of silicon in the matrix can be determined. The values of kT/W_e are plotted against $1/T$ in Fig. 13 and from the slope of the resulting straight line, the value of Q is found to be 60.8 kcal/mole. This agrees very well with the value of Q determined from the coarsening kinetics. The values of $\bar{a}_o$ and k are

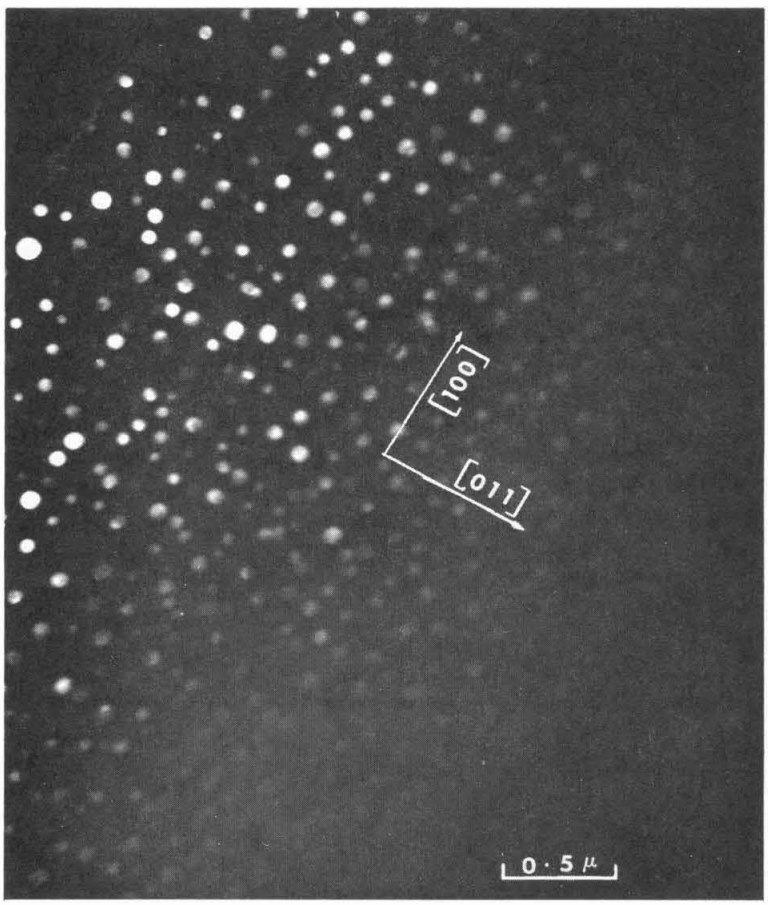

Fig. 8. Dark-field electronmicrograph of Ni-6.5 wt% Si alloy aged for 30 minutes at 775°C.

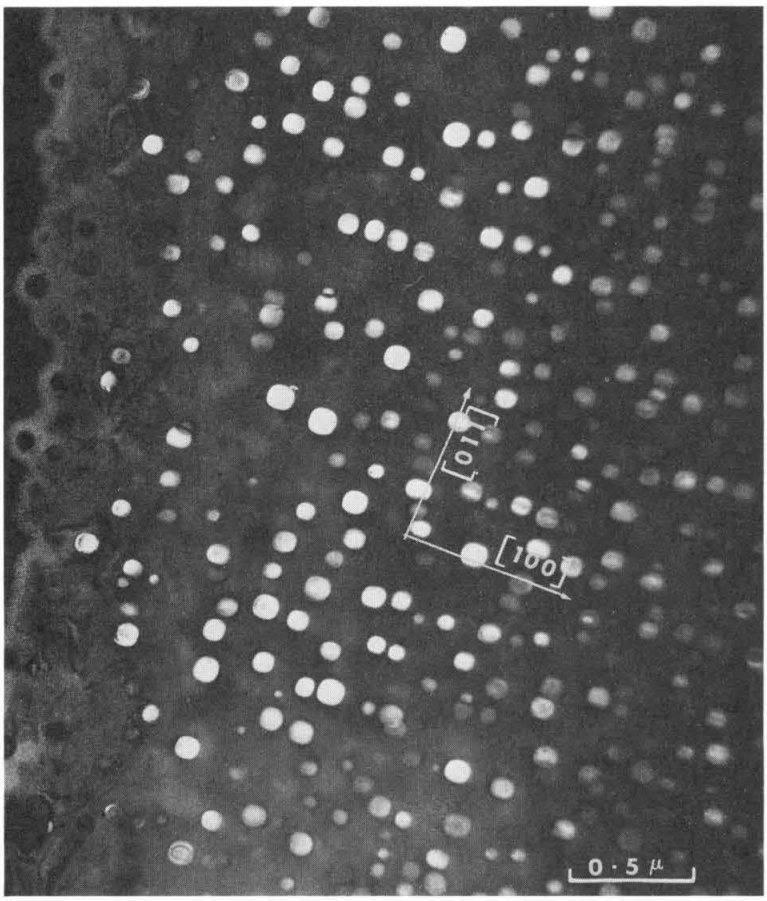

Fig. 9. Dark-field electronmicrograph of Ni-6.5 wt% Si alloy aged for 1-1/4 h. at 775°C.

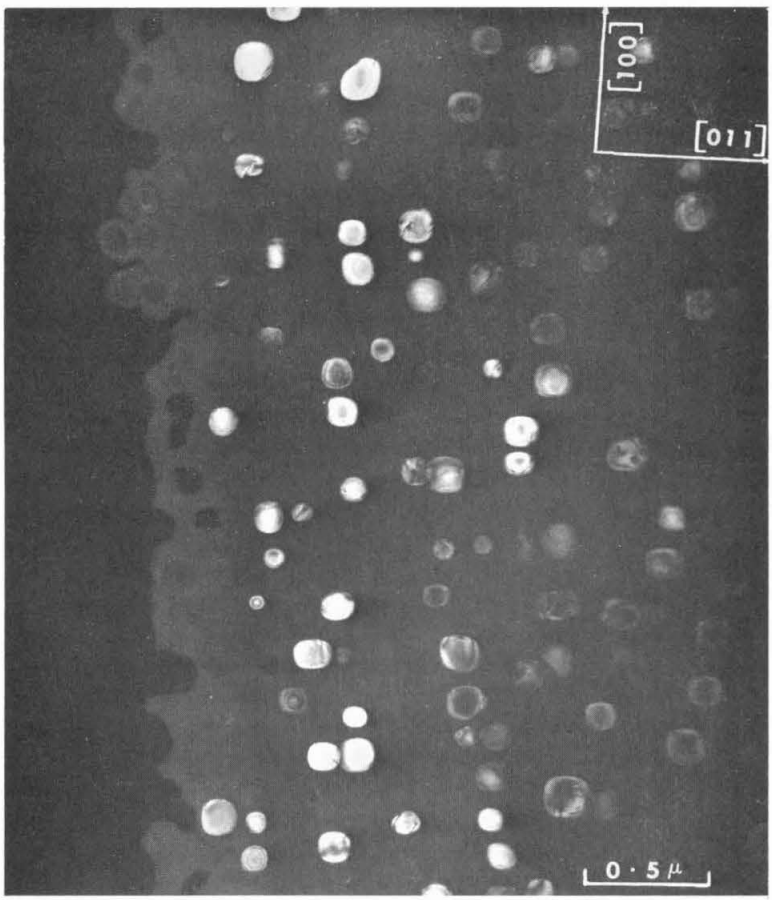

Fig. 10. Dark-field electronmicrograph of Ni-6.5 wt% Si alloy aged for 5 h. at 775°C.

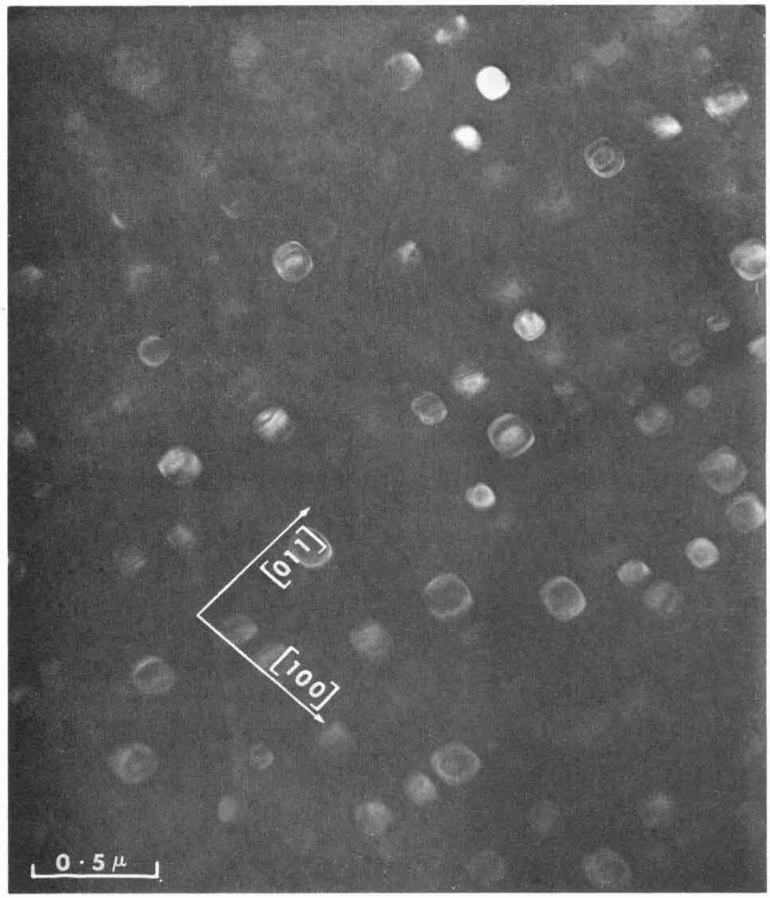

Fig. 11. Dark-field electronmicrograph of Ni-6.5 wt% Si alloy aged for 8 h. at 775°C.

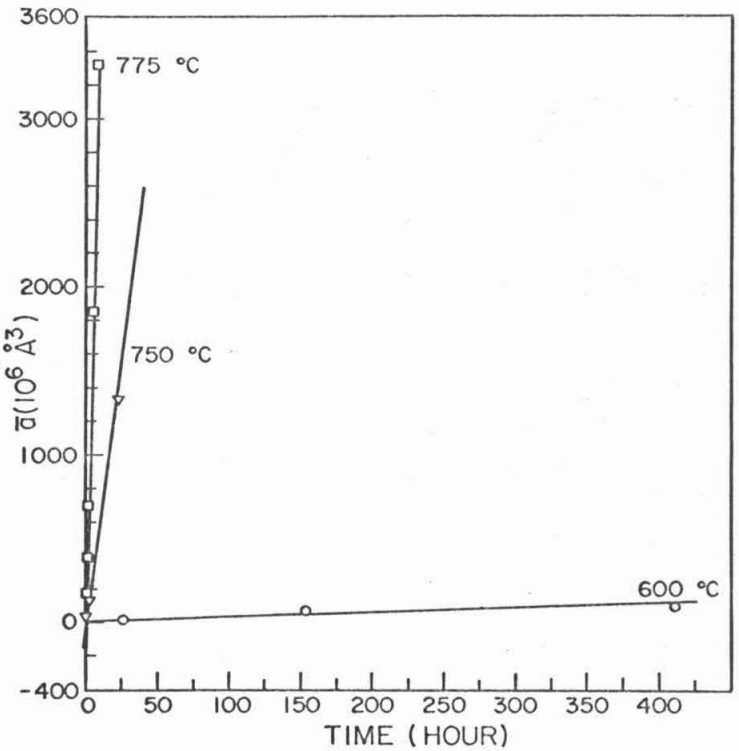

Fig. 12. Cube of mean particle size $\bar{a}^3$ against t. Data for 750°C and 600° are from Hornbogen and Roth (6).

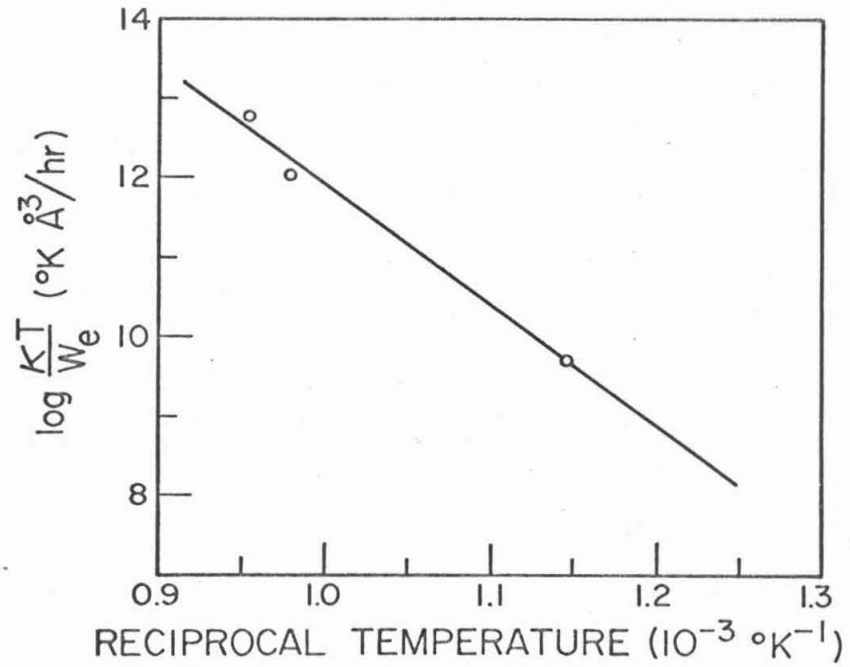

Fig. 13. Determination of the activation energy for the coarsening of γ' by an Arrhenius plot of the rate constants K compensated for the temperature dependent factor T/W_e.

TABLE II

EXPERIMENTALLY DETERMINED VALUES OF THE RATE CONSTANTS K, THE INTERFACIAL ENERGIES γ AND THE MEAN INITIAL PARTICLE SIZES $\bar{a}_o$.

Aging Temp. T (°C)	Rate Constant K (A^3/h)	Mean Initial Particle Size, $\bar{a}_o$ (A)	Interfacial Energy γ ($ergs/cm^2$)
600	3.0×10^5	2.0×10^2	13.0
750	6.6×10^7	-5.19×10^2	10.5
775	4.0×10^8	-6.97×10^2	11.5

reported in Table II. The value of activation energy agrees with the value of Q namely 61.7 kcal/mole, determined by Swalin and Martin.[7]

C. Time dependence of the volume fraction

The volume fraction of γ' precipitates at different aging times is calculated from the measured values of silicon content in the matrix with the aid of Eq. (9). The values of Φ are plotted against $t^{-1/3}$ at different temperatures in Fig. 14 and a linear relation is observed. This behavior is consistent with Eq. (11). The change in volume fraction of precipitate during coarsening is very small compared with that which occurs during precipitation. Cohen and Fine[8] have also shown that the volume fraction does change with time. It is now apparent from the experimental results that the constancy of the volume fraction of precipitate is not a valid criterion for particle coarsening.

D. Distribution of particle sizes

Dark field micrographs of specimens aged for 30 minutes, 1-1/4 hours, 5 hours and 8 hours at 775°C are shown in Figs. 8 to 12. The γ' particles are distributed randomly at the beginning of aging, but later on tend to align along the ⟨100⟩ direction. The edge length a, of 400 cuboidal shape γ' particles, was measured along the [100] direction and placed into a number of suitable size intervals. The average particle sizes $\bar{a}$ were calculated from each histogram and were then normalized according to a previously used procedure[9] for comparison with the theoretical distribution predicted by the Lifshitz-Wagner analysis. The unnormalized histogram g (a, t) is multiplied by $9/4\ \bar{a}$ to get a normalized histogram. They are plotted against the

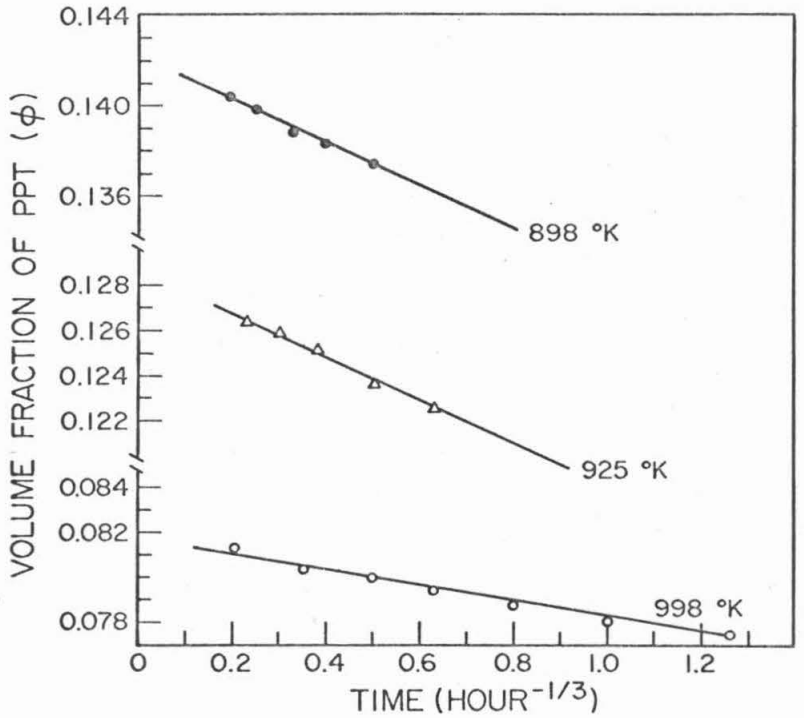

Fig. 14. Volume fraction Φ of γ' precipitate vs.$t^{-1/3}$ during coarsening in Ni-Si alloys.

normalized particle size $\rho = a/\bar{a}$ in Figs. 15 to 18. The theoretical distribution $\rho^2 h(\rho)$ is also shown for comparison.

The histograms are generally broader than the theoretical curve and the cutoff occurs in the neighborhood of $\rho = 1.6$ to 1.7. Although the maxima for experimental histograms never reach the maximum of theoretical curve, their positions are in the neighborhood of the theoretical maximum. It is evident from Figs. 15 to 18 that the deviation of the experimental cutoff values from the theoretical one is reduced as the aging proceeds, and after 5 hours of aging both values are approximately the same. Thus the systematic change of histograms with time indicates that steady state size distributions are attained at the end of the aging treatments.

E. The γ'-matrix interfacial energy

The only unknown parameters in Eqs. (13) and (7) are D and γ. Two new equations[10] are defined such that

$$\alpha = (k/\eta)^{1/3} = \frac{4\gamma C_e V_m}{R T} \tag{14}$$

and

$$\beta = (k^2 \eta)^{1/3} = (4/9)\, 4\, D\, V_m \tag{15}$$

Since α and β are determined from the experimental values of k and η we can solve for γ and D from Eqs. (14) and (15). The values of W_e were converted to molar concentrations (mole/cm^3) by using the relation $C_e = \rho_x W_{si}/M_{si}$. Where ρ_x is the density of the Ni-solid solution with weight fraction W_{si} of Si, M_{si} is the atomic weight of Si and in this case ρ_x was assumed to be equal to ρ_{ni}. The molar volume V_m is calculated from the relation $V_m = Na^3$, where N is Avagadro's number

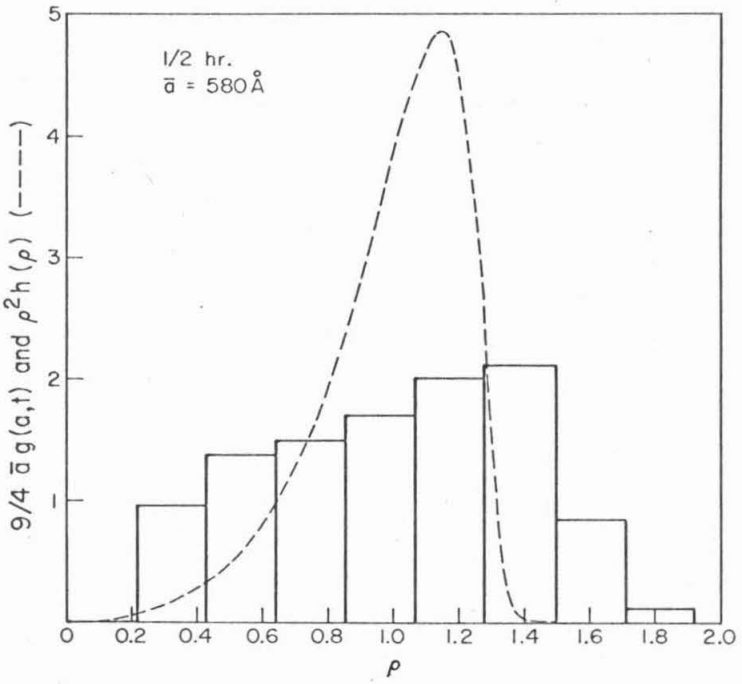

Fig. 15. Experimentally determined particle sizes distribution (solid lines) after aging for 1/2 h. at 775°C. The dashed line is theoretical.

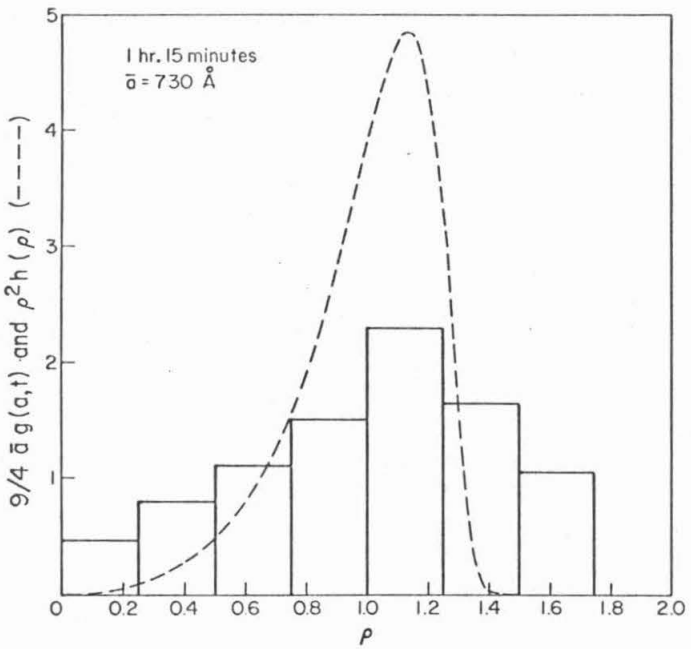

Fig. 16. Experimentally determined particle sizes distribution (solid lines) after aging for 1 1/4 h. at 775°C. The dashed line is theoretical.

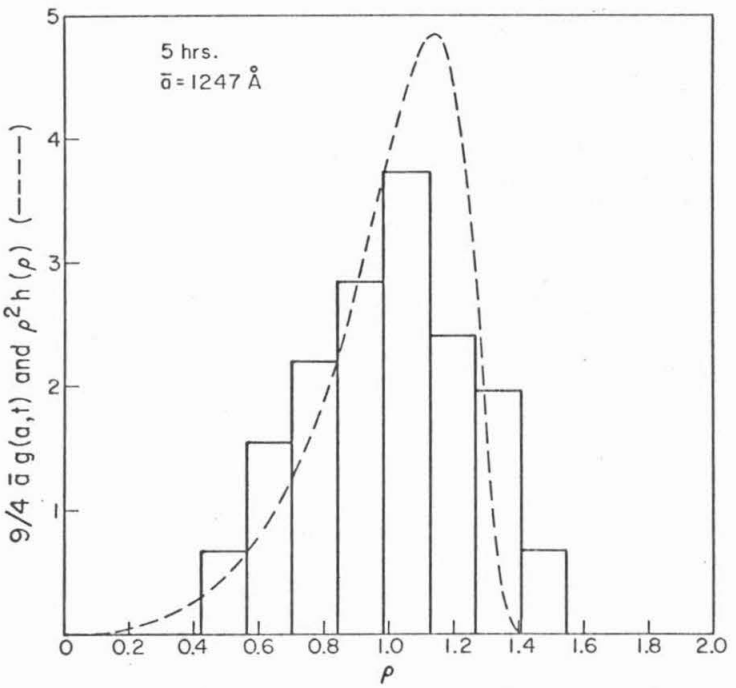

Fig. 17. Experimentally determined particle sizes distributions (solid lines) after aging for 5 h. at 775°C. The dashed line is theoretical.

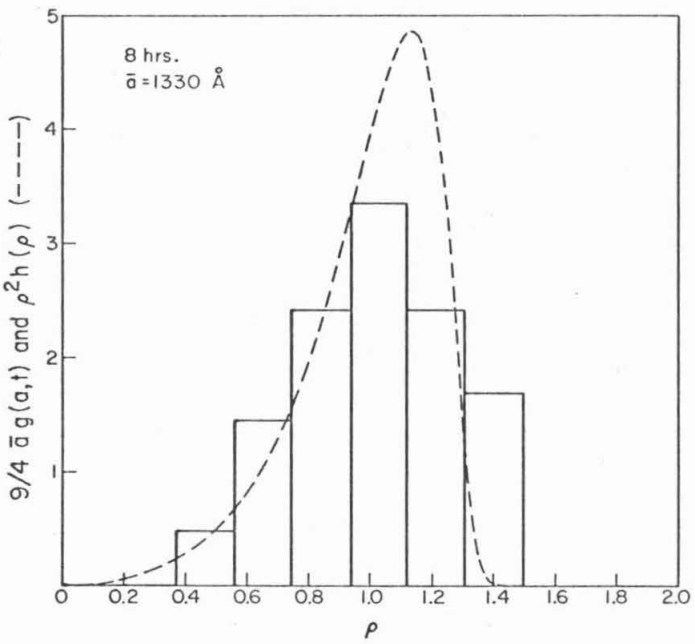

Fig. 18. Experimentally determined particle sizes disbribution (solid lines) after aging for 8 h. at 775°C. The dashed line is theoretical.

and a is the lattice parameter of the unit cell of $Ni_3 Si$. The value is found to be 25.16 cm^3/mole. Since the interfacial free energy γ is a function of orientation, the values of γ along the [100] direction were calculated. The estimated values of γ are reported in Table II. These values are found to be independent of temperature within experimental errors, and are quite comparable to those in Ni-Al[11] and Ni-Ti systems.[4]

F. Diffusion coefficient of the solute in the matrix

Although Wagner's theory is applicable only to the coarsening of a precipitate in fluid matrices, it can also be applied to solid systems provided D is replaced by D_{eff}. The value of D_{eff} incorporates the effects of volume and compositional constraints, but may also include numerical factors that become important if the diffusion field around each particle is not spherically symmetric. Keeping this in mind, the value of k and η have been determined at different temperatures. Using Eq. (15) and knowing the value of V_m = 25.16 cm^3/mole, the values of D_{eff} are calculated. These values are reported in Table III and are compared with the values of D_{si} obtained from Swalin's data.[7] These two values differ by one order of magnitude.

G. Loss of coherency

Fig. 7 shows the sudden change in the concentration of silicon in the matrix for specimen aged at 775°C. This sudden change is probably due to the loss of coherency of the γ' particles. In an effort to understand this phenomenon, transmission electromicroscopy was performed on specimens aged for different times. Dislocations were

first observed at the γ'- matrix interface in a sample aged for 16 hours at 775°C. Further aging resulted in the formation of distinct dislocation networks as shown in Figs. 19 to 21. According to Weatherly and Nicholson[12] similar types of dislocation networks were formed at γ' interfaces in Ni-Cr-Al alloy. The misfit energy was thus released due to the formation of dislocations at interfaces and particles became semi-coherent. Symmetrical hexagonal dislocation networks were observed after aging the specimen for 238 hours at 775°C. The formation of this kind of network was inferred from the work on nimonic 80A alloy.[12] Unfortunately, no attempts were made to determine the nature of the interfacial dislocations. The mechanism for the loss of coherency was studied by deforming a specimen aged for 14 hours at 775°C. It is evident from Figs. 22 and 23 that particles after one hour of aging time had many dislocations at interfaces as opposed to an undeformed sample aged for the same time, shown in Fig. 24.

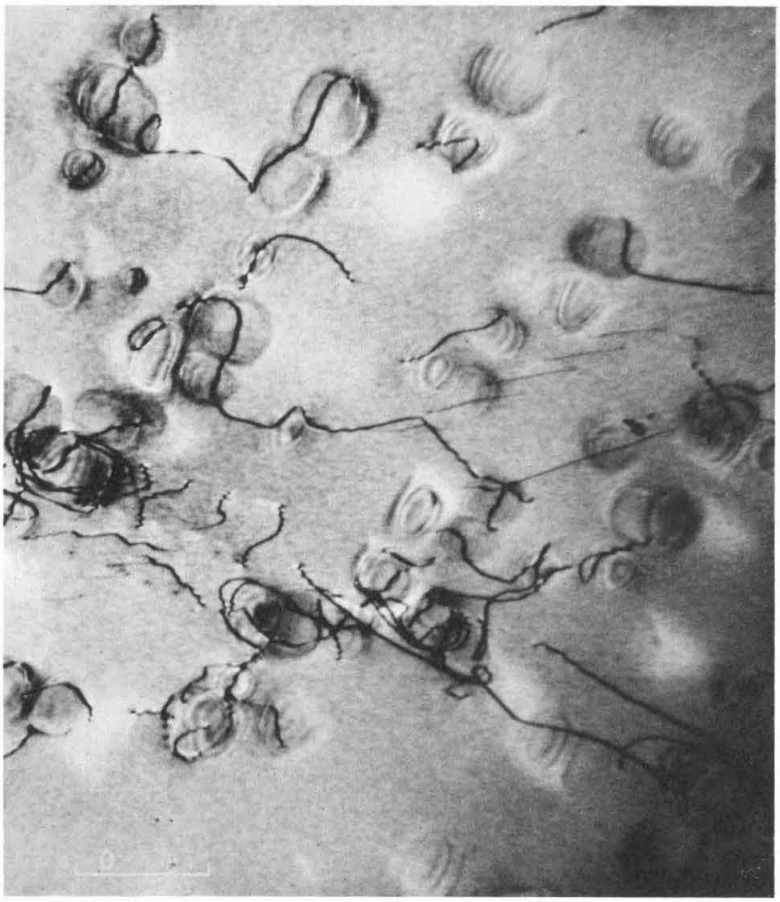

Fig. 19. Networks of dislocations on γ' particles in Ni-6.5 wt% Si alloy aged for 32 h. at 775°C.

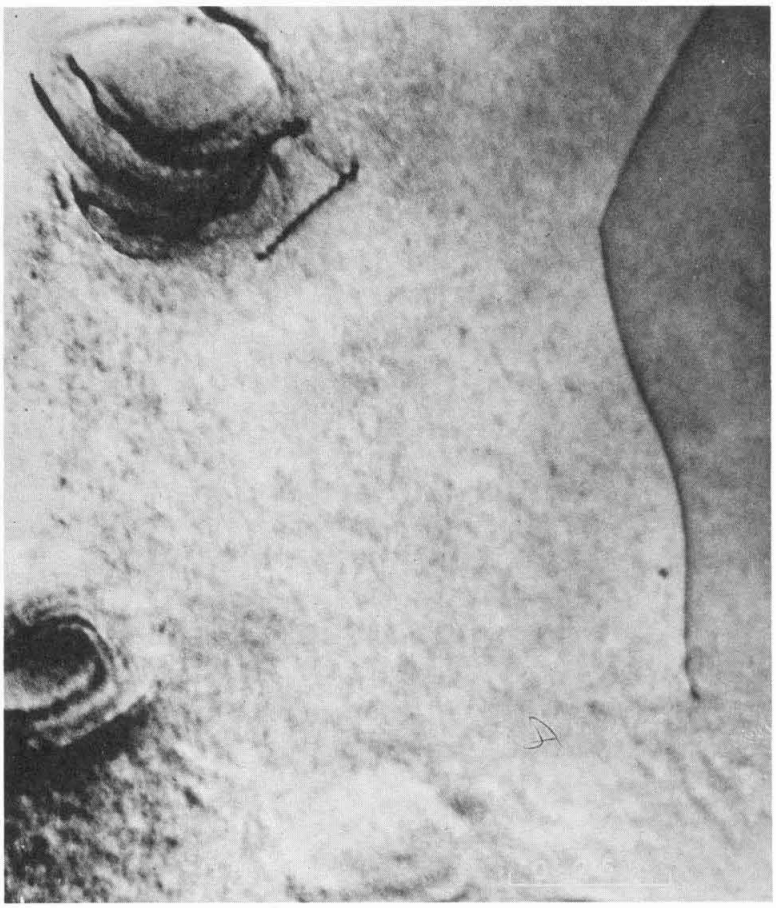

Fig. 20. Dislocations on γ' particles in Ni-6.5 wt% Si alloy aged for 133 h. at 775°C.

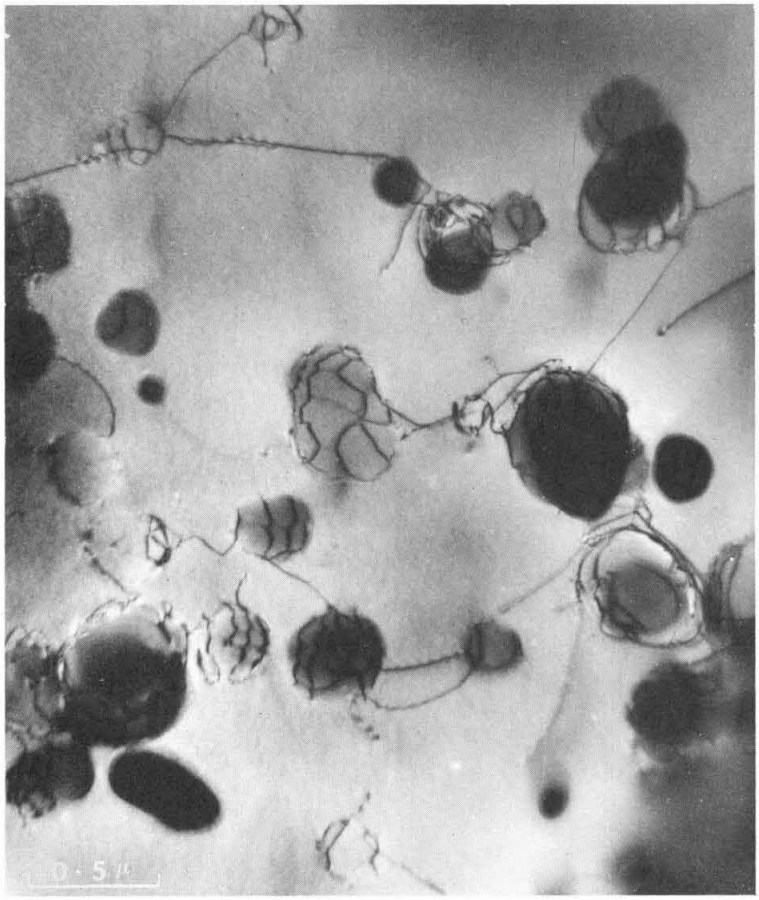

Fig. 21. Hexagonal networks of dislocations on large γ' precipitates in Ni-6.5 wt% Si alloy aged for 238 h. at 775°C.

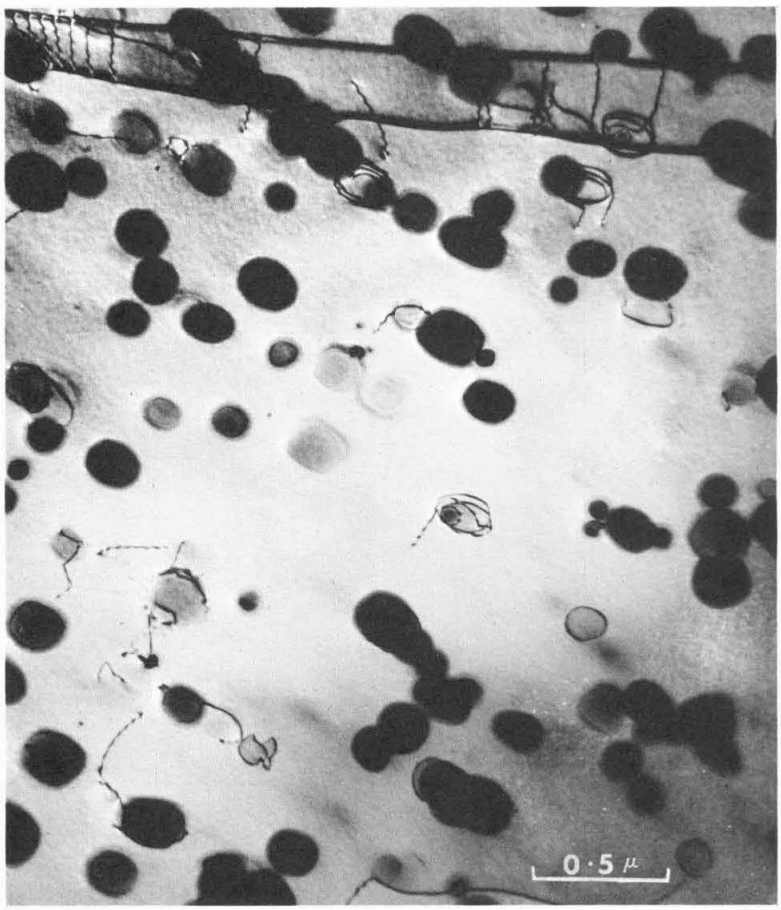

Fig. 22. Dislocations on γ' particles in Ni-6.5 wt% Si alloy aged for 1 h. at 775°C after 2% deformation.

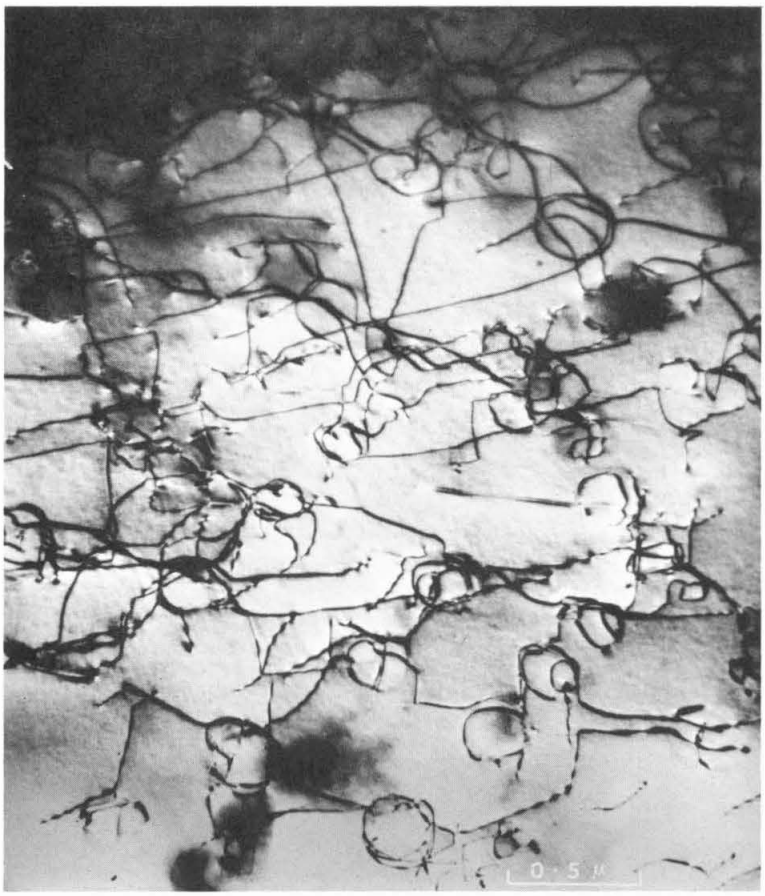

Fig. 23. Dislocations on γ' particles in Ni-6.5 wt% Si alloy aged for 1 h. at 775°C after 5% deformation.

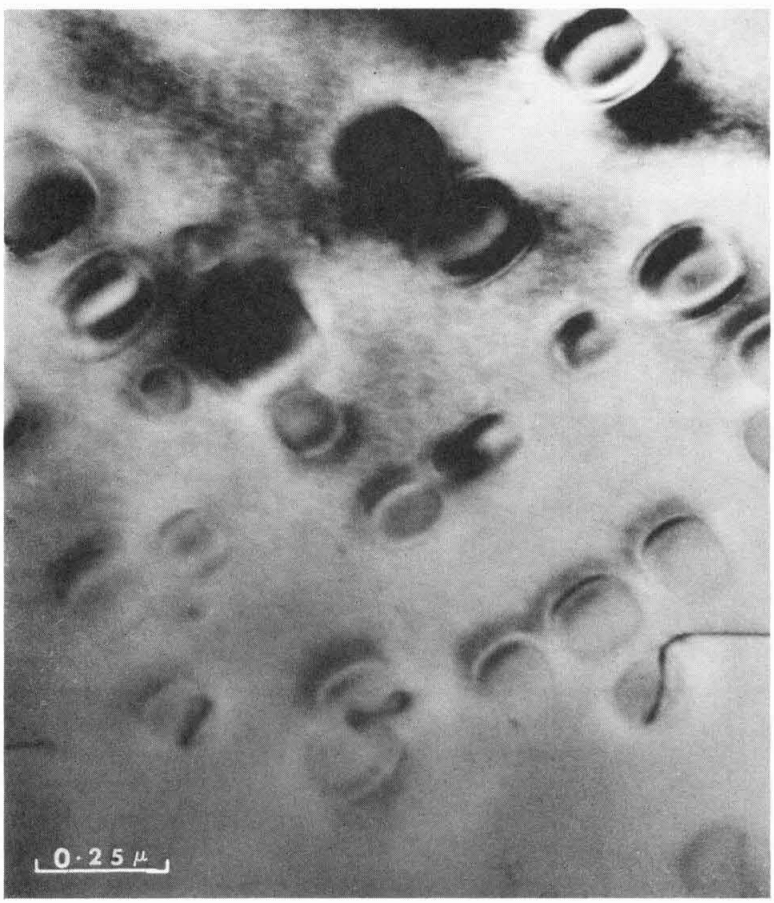

Fig. 24. Bright-field electronmicrograph of Ni-6.5 wt% Si alloy aged for 14 h. at 775°C.

I. V. DISCUSSION

A. Equilibrium solubility

The values of silicon content in the matrix calculated from aging experiments at $t = \infty$ truly represent coherent equilibrium solubilities, as shown from the result of the dissolution experiments.[13] These values are slightly greater than Hansen's[5] data and are justified on the basis of Cahn's theory. According to Cahn[14] and Oriani,[15] the coherent solubilities are always greater than the incoherent ones, and the magnitude of the difference is related to the lattice misfit.

In Ni-Si alloys the γ' precipitates are perfectly coherent with the matrix and the fractional misfit $\Delta a/a$ between the unstrained lattices of the precipitate and the matrix is -0.3%[16] The extent to which solid solution is stabilized by coherency strains depends largely on the lattice misfit. Since $\Delta a/a$ in the Ni-Si system is fairly small, the coherent solubility of γ' is probably not much greater than the incoherent solubility. On the other hand, the values of lattice misfit in Ni-Al and Ni-Ti are 0.4 and 0.9 respectively and their effects are reflected in significant differences between the values of coherent and incoherent solubility.[13] Assuming that Hansen's curve represents the incoherent solubility of γ' in Ni-Si, our coherent solubility data are consistent with theoretical predictions, insofar as they are displaced to slightly higher concentration.

Plastic deformation seems to be responsible for the abrupt change in silicon concentration in the matrix for the specimen aged at 652°C. It contributes to a rapid increase of dislocation density in the

matrix and γ' precipitates become incoherent due to the formation of dislocation networks at interfaces. The lattice misfit energy is thus relieved. Fig. 5 shows that γ' particles practically remained coherent after deforming by 25% at 625°C, indicating no sudden change in silicon content of matrix upon further aging.

B. Kinetics of particle growth

The plot of $\bar{a}^3$ versus t in Fig. 13 shows that Eq. (12) is obeyed, and is thus consistent with the theories of coarsening presented by Lifshitz and Slyzov[1] and Wagner,[2] in which large particles grow at the expense of small ones by a diffusion controlled mechanism. Time t in Eq. (12) is measured from the beginning of coarsening; time τ needed for precipitation is neglected. This does not affect the value of k but lowers the value of $\bar{a}_o^3$ by an amount $k\tau$. The value of a_o can be negative, depending upon the time law for precipitation. The presence of coherency stress in Ni-Si system, similar to that in Ni-Al and Ni-Ti systems,[4] does not seem to violate the coarsening kinetics predicted by the Wagner and Lifshitz theory. Therefore, it does not seem to be critical for the success of the theory.

C. Distributions of particle sizes

It is clear from Figs. 15 to 18 that the experimental particle size distributions change systematically with time, indicating that steady state distribution is achieved at longer aging times. Although Wagner's theory is only applicable to the coarsening of stress free particles in matrices, it is found to be valid for Ni-Si system with lattice, a misfit of -0.3%. The cutoff value of ρ for experimental distributions in Ni-Si systems do not differ as much from the

theoretical value as for Ni-Al and Ni-Ti systems.[4] In fact, the experimental cutoff value for Ni-Cr-Al system[6] does coincide with the theoretical value. The magnitude of deviation is related to the degree of lattice misfit present in these systems. The plot of deviation $(\rho_{exp}-\rho_{th})/\rho_{th}$ versus lattice misfit $\Delta a/a$ in Fig. 25 indicates that larger misfit contributes to larger deviation of experimental value of ρ cutoff from the theoretical one. For Ni-Cr-Al with 0.01% misfit, it is zero, whereas for Ni-Ti system it is 40% Therefore, it can be safely said that the disagreement between experiment and theoretical distribution of particle sizes is primarily due to the presence of lattice misfit. The requirement of small volume fraction of γ' precipitate during coarsening suggested by Wagner's theory is satisfied in Ni-Si systems, since the aging temperature (775°C) was high enough. There are other factors which perhaps affect the size distribution of the particles, namely

(1) Diffusion through stress fields.

(2) The anisotropy of the interfacial energy as well as elastic constants of the matrix and the particles.

(3) The stress field set up by the interaction of particles when the average interparticle separation is smaller than the mean particle size.

The experimental maxima never attain the value of the theoretical maximum and this discrepancy may be explained by taking into account the above mentioned facts, which seem to complicate the coarsening kinetics.

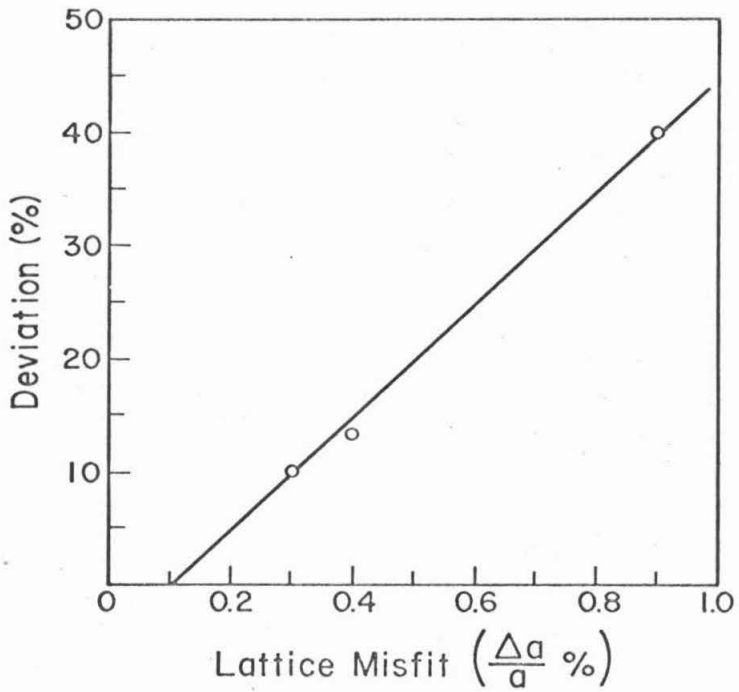

Fig. 25. Plot of (ρexp - ρth) / ρth vs. lattice misfit, Δa/a for Ni-Al, Ni-Ti and Ni-Si alloys.

D. The γ'-matrix interfacial energy and effective diffusion coefficient

The equations for the coarsening of precipitates in fluid matrices may be applied to solid systems with certain modifications: (i) γ is replaced by $\gamma(\hat{n})$, which is the interfacial tension of a surface element whose orientation is specified by the unit normal $\hat{n}$, and r is replaced by $\lambda(\hat{n})$ which is the distance from the center of inversion symmetry of the equilibrium body to the plane tangent to the surface element of orientation $\hat{n}$; (ii) D is replaced by D_{eff} which takes into account the effects of volume and compositional constraints, along with other factors if diffusion field around each particle is not spherically symmetrical. Therefore, the interfacial energy (γ) is measured along [100] direction and found to be independent of temperature. The accuracy of our calculated value of γ cannot be estimated due to the lack of experimentally determined value of γ for Ni_3Si-matrix interface. It is known, however, from theoretical considerations[9] that the {100} interface between pure nickel and stoichiometric γ' precipitate has approximately zero interfacial free energy. Allowing for deviations from stoichiometry in γ' and for the concentrations of Si in the Ni-rich matrix, the low values of γ(10-13 ergs/Cm^2) must be considered satisfactory. Fortunately, similar values of γ(13-14 ergs/Cm^2) for Ni-Al and Ni-Ti[18] systems have been reported and interpreted using the same arguments.

The numerical factor (4/9) in Eq. (15) comes from the theoretical distribution of particle sizes.[1, 2] This factor is only valid for those systems where experimental distribution of particle sizes matches with the theoretical distribution. If this condition is not satisfied, coarsening kinetics will be affected.

The distribution of particle sizes during coarsening of the γ' precipitate in Ni-Si system deviates very little from the theoretical distribution and furthermore this deviation becomes negligible at longer aging times. The values of D_{eff} calculated from Eq. (15) are about a factor of 10 greater than D_{si}, taken from the extrapolated data of Swalin and Martin at high temperatures. This slight deviation seems to have insignificant effect on D_{eff}, and it cannot account for the large discrepancy between D_{eff} and D_{si}. The values of D_{eff} predicted by the application of irreversible thermodynamics to the coarsening of γ' coherent precipitate, are calculated from the relation,[11]

$$(D_{si})_{eff} = \frac{X_{ni} D_{si} D_{ni} (1+X_{si}/X_{ni})}{X_{ni} D_{ni} + X_{si} D_{si}} \qquad (16)$$

where the X's represent mol fractions of the components in the matrix and the D's refer to the diffusivities of Si and Ni in the matrix. Eq. (16) is only valid for the volume constraint that arises from the need to remove a volume of matrix materials around a growing particle equal to the volume by which the particle has grown in order to avoid any elastic strain energy in the system. For an accurate comparison between experimental values of D_{eff} and derived from Eq. (16), we must know D_{si} and D_{ni} as functions of the silicon content of the matrix. Due to the lack of these data, they were estimated by assuming that the activation energies are proportional to the solidus temperature at different concentrations. The frequency factor that appears in front of exponential term in the diffusion equation is considered to be

independent of temperature. D_{si} and D_{ni} were calculated from the data of Swalin[7] and Hoffman[19] respectively. These values were then substituted into Eq. (16) to determine $(D_{si})_{eff}$.

The values of $(D_{si})_{eff}$ reported in Table III agree quite satisfactorily with the experimental values of D_{eff}. Thus foregoing approximation for the calculation of D_{si} and D_{ni} seems to be quite justified. Probably the discrepancy by a factor of 10 between D_{eff} and D_{si} arises from the fact that the effect of concentrations of silicon on D_{si} were neglected. The values of D_{si} are only valid for dilute solute concentrations.

The quantitative agreement between the experimental and calculated values of D_{eff} indicates that the influence of volume constraints on effective diffusion coefficient of silicon in the matrix are quite pronounced. The principle of minimum entropy production, thus, seems to offer plausible explanations only for the Ni-Si system but not for Ni-Al and Ni-Ti[4] systems.

E. The role of strain energy and of elastic interaction between particles

The Lifshitz-Wagner theory is applicable only to spherical particles coarsening in a fluid matrix. In the present investigation particles are spherical at the early stages of aging and later on they become cuboidal in shape. It has been observed in Fe-Ni-Cr-Ti system[20, 21] that γ' particles exist as spherical particles when the lattice misfit with the matrix is less than 0.1% When the misfit is greater than 0.1% as in Ni-Si system (-0.3%), Ni-Al (0.4%) and Ni-Ti (0.9%) the γ' particles appear as cubes. The change in particle shape from sphere to cube is due to the appropriate balance between strain energy and

TABLE III

VALUES OF THE VARIOUS DIFFUSION COEFFICIENTS ASSOCIATED WITH THE COARSENING OF THE γ' PRECIPITATE IN Ni-Si ALLOYS

Aging Temp. T (^{o}C)	Effective Diffusion Coeff. D_{eff} (Cm^2/Sec)	Expt. Diffusion Coeff. of Si, D_{si}^{*} (Cm^2/Sec)	Theoret. Effective Diffusion Coeff. of Si, D_{eff} (Cm^2/Sec)
600	2.13×10^{-15}	4.52×10^{-16}	3.02×10^{-15}
750	5.0×10^{-13}	8.55×10^{-14}	4.84×10^{-13}
775	1.87×10^{-12}	1.84×10^{-13}	1.1×10^{-12}

* Value of experimental diffusion coefficient of s_i obtained from Swalin et al[7]

surface energy. Therefore, the equilibrium shape is influenced by the strain energy consideration. It may also, however, be a function of particle size. It has been demonstrated[22] that the γ' particles in Ni-Al alloys tend to align along [100]. This is attributed to the elastic interactions between the particles. Similar hypothesis can be used to explain the alignment process in the Ni-Si alloy. It is observed that in the Ni-Si system aligned particles grow at the expense of the unfavorable situated particles. This is very similar to what is seen in Ni-Al alloy. Since the strain energy in the Ni-Si system is lower than in Ni-Al, the degree of alignment is not very pronounced. The coarsening kinetics of γ' particles seem to be unaffected by elastic interactions of particles.

F. Mechanism of loss of coherency

The loss of coherency of a growing particle can occur by any of three possible mechanisms: (a) the coherency stresses in the matrix due to misfit result in the punching of dislocation loops at or close to the particle-matrix interfaces; (b) the climb of dislocations from a source in the matrix to the particle-matrix interface. The elastic interaction between the strain fields of the particle and of the dislocation provides the driving force for climb; (c) the nucleation of dislocation loop inside the particle due to the presence of its own stress field. This is most likely to happen in particles in which the composition deviates from stoichiometry.

In the Ni-Si system the γ' particles are nearly spherical and are in a state of pure dilation. The transformation strain e^T is given by

$$e^T = \sum_{i=1}^{3} e_{ii}^T = 3 \times 0.003 = 0.009 \qquad (16)$$

For spherical particles in pure dilation, the critical value of the strain for dislocation punching is given by $e^T_{critical} \geq .014$[23] and thus no punching of loops would be expected for γ'. Therefore, in this case mechanism (a) will not be operative to cause loss of coherency. The mechanism (c) is also forbidden because of the requirement of large stress for the nucleation loops inside the γ' particles. The only plausible mechanism for loss of coherency is through the supply of dislocations at the γ'-matrix interfaces by a climb process. An example of semi-coherent precipitate is given in Fig. 21, for specimens aged for 238 hours at 775°C. A very few γ' particles have lost coherency, while others are still fully coherent, having a few dislocation loops at the interfaces.

From the energy consideration, Brown and Woolhouse[24] have shown that the loss of coherency of γ' particle is related to its radius. Two different radii have been defined. The critical radius $r_{critical}$ is the radius below which the particle will not sustain dislocation loops. Another radius r* is the one at which the precipitate lowers its energy by having a loop at its interface. For a precipitate of radius r such that $r_{critical} < r < r^*$, having a dislocation loop at the interface, will grow coherently at the expense of the incoherent ones because of the metastability of the incoherent state with respect to the coherent state. In the same way, for a precipitate of radius r such that $r > r^*$, it will transform to a partially incoherent state.

Using Eqs. (5) and (6) of Brown and Woolhouse[24] and taking $\nu = 0.33$, $b = 2.47$ Å and $\epsilon = 0.002$ for Ni-Si system, the values of $r_{critical}$ and r* are calculated. The shear moduli of the precipitate and the matrix are taken to be the same. The radius of loop is also assumed to be the radius of the particle. Under these conditions the values of $r_{critical}$ and r* are 270 Å and 520 Å respectively. The experimental mean value of $r_{critical}$ is found to be 375 Å. In view of all the simplified assumptions, the experimental result is in good agreement with the theoretical value. The radius of the γ' precipitate after aging for 238 hours at 775°C is found to be 1250 Å. Thus the experimentally observed r* is about twice the theoretically determined value. The discrepancy may be due to oversimplified assumptions.

In order to test the mechanism for loss of coherency of γ' precipitate, the specimens were first aged for 14 hours and then deformed by 2% and 5%. Later on, these specimens were further aged and bright field electronmicrographs were taken. It was observed that the plastically induced dislocations in the matrix were attracted to the γ' matrix interfaces. The loss of coherency was experimentally shown to occur at a smaller radius as compared to the radius of the γ' precipitate in an underformed specimen under identical conditions. Thus it seems that the high density of dislocations in the matrix is solely responsible to transform a coherent γ' precipitate into a semi-coherent state by a climb process.

I. VI. SUMMARY AND CONCLUSIONS

A linear variation in silicon concentrations with $t^{-1/3}$ during the coarsening of γ' precipitate in Ni-6.5 wt. % alloy confirms the validity of Lifshitz and Wagner theory.[1, 2] The equilibrium coherent solubilities of silicon in the matrix are estimated to be approximately 5% greater than the values reported by Hansen.[5] The experimentally determined average particle size $\bar{a}$ follows the coarsening kinetics of particle growth[1, 2] as a function of $t^{-1/3}$. The values of activation energy determined from the slopes of rate-constants vs. 1/T curves are in excellent agreement. The volume fraction of γ' precipitate during the coarsening process changes as a function of time, and thus it contradicts the assumption made in Lifshitz-Wagner theory.

The experimental particle-size distributions are broader than the theoretical distribution in the early stages of aging. But at a later stage both of them become identical, except for the large difference in their maxima. It is suggested that this discrepancy is due to the lattice misfit (-0.3%) in the Ni-Si alloy. The values of interfacial energy, γ, is found to be 12 ergs/Cm^2 and matches satisfactorily the reported data for γ in Ni-Al and Ni-Ti alloys. Taking into account the effect of silicon content on the activation energy for diffusion, it appears that the values of D_{eff} of silicon predicted by irreversible thermodynamic principle of minimum entropy production are in quantitative agreement with the experimental results.

The γ' particles become semicoherent after a long aging time at 775°C. The loss of coherency is related to the formation of hexagonal networks of dislocations at the γ'-matrix interfaces by a climb process. A large amount of plastic deformation also causes particles to become semi-coherent.

REFERENCES

1. I. M. Lifshitz and V. V. Slyzov, J. Phys. Chem. Solids, 19, 35 (1961).
2. C. Wagner, Z Electochem 65, 581 (1961)
3. C. Y. Li and R. A. Oriani, Proc. Bolton Landing Conf. on Oxide Dispersion Strengthening (1966).
4. A. J. Ardell, Metallurgical Transactions (Accepted for Publication).
5. M. Hansen and K. Anderko, Constitution of Binary Alloys, 2nd edition, p. 1040, McGraw-Hill (1958).
6. V. E. Hornbogen and M. Roth, Z. Metallkunde, 58, 842 (1967).
7. R. A. Swalin and A. Martin, Trans. Am. Inst. Min. Metall. Engrs. 206, 567 (1956).
8. J. B. Cohen and M. E. Fine, Scripta Met 2, 153 (1968).
9. A. J. Ardell and R. B. Nicholson, J. Phys. Chem. Solids 27, 1793 (1966).
10. A. J. Ardell, Acta. Met, 15, 1772 (1967).
11. A. J. Ardell, Acta. Met, 16, 511 (1968).
12. G. C. Weatherly and R. B. Nicholson, Phil. Mag. 17, 801 (1968).
13. P. K. Rastogi and A. J. Ardell, Acta. Met, 17, 595 (1969).
14. J. W. Cahn, Acta. Met, 14, 83 (1966).
15. R. A. Oriani, Acta. Met, 14, 84 (1966).
16. H. Gleiter and E. Hornbogen, Mat. Sci. and Eng. 2, 285 (1968).
17. C. A. Johnson, Surface Sci. 3, 429 (1964).
18. A. J. Ardell, Int. Symp. on Mechanism of Phase Transformation, Manchester, (1968).

19. R. E. Hoffman, F. W. Pikus and R. A. Ward, Trans. Am. Inst. Min. Metall. Engrs. 206, 483 (1956).

20. A. Kelley and R. B. Nicholson, Progress in Materials Science, 10, 149, Pergamon Press, Oxford (1963).

21. M. J. Blackburn, Ph. D. Dissertation, University of Cambridge (1961).

22. A. J. Ardell and R. B. Nicholson, Acta. Met, 14, 1295 (1966).

23. C. G. Weatherly, Phil. Mag., 17, 791 (1968).

24. L. M. Brown, G. R. Woolhouse and U. Valdré, Phil. Mag., 17, 781 (1968).

PART II. RATE OF CRYSTALLIZATION OF AN AMORPHOUS Fe-P-C ALLOY

II. I. INTRODUCTION

In recent years, several experimental techniques have been developed to produce alloys in a non-crystalline state. Methods such as high vacuum vapor deposition are used extensively to obtain amorphous metallic thin films.[1] Rapid quenching from the liquid state can also be used to obtain amorphous alloys.[2] The foils obtained by this technique are about 5-50 μ thick, compared with about 0.2μ for vapor deposited films. As a result, the study of their structure by x-ray diffraction, and the measurements of the electrical and magnetic properties are greatly simplified. With this technique, amorphous binary alloys have been obtained in Au-Si,[3] Pd-Si[4] and in Te base alloys containing Ge, Ga and In.[5, 6] More recently ternary amorphous alloys containing Fe, P and C have been reported[7] around the composition Fe_{75}-P_{15}-C_{10}, the subscripts denoting the atomic concentrations of the elements. The atomic arrangement in the Fe-P-C amorphous alloys has been described in Ref. (8) and some of their electrical and magnetic properties have been reported.[9, 10] These alloys are obviously metastable and transformed into the stable crystalline state as the temperature is increased. The present investigation is concerned with the rate of transformation from the amorphous to the crystalline state.

II. II. EXPERIMENTAL TECHNIQUES

Ternary alloys of Fe-P-C were prepared from pure iron powder (99.99%), pure red phosphorus powder and carbon powder obtained from spectroscopic grade graphite electrodes. The three powders were thoroughly mixed and pressed in a rectangular steel die (1 x 3/8 x 1/4") at a pressure of 50,000 lbs/in^2. These compacts were sintered in two stages to allow the formation of iron phosphides by solid state reaction at low enough temperature so as to avoid volatilization of phosphorus. Samples placed in evacuated pyrex tubes were slowly heated up to 580°C in about 70 hours and kept at this temperature for about 40 hours. The samples were then transferred to evacuated quartz tubes and heated slowly up to 900°C and maintained at this temperature for 40 hours. The sintered compacts were then melted in a quartz crucible in an argon atmosphere and the melted alloys were cast in the form of rods by sucking the melt into quartz tube of 2 mm diameter.

Quenching from the liquid state was achieved by the "piston and anvil" technique.[11] The resulting foils are about 20 mm in diameter and 40 to 50μ thick. The average rate of cooling is of the order of 10^5 °C/sec.[12] A number of samples were chemically analyzed by both wet chemistry and electron microprobe analysis. The average chemical analysis in at.% was 74.9 ±1% Fe, 15.0 ±1% P and 10.0 ±0.5% C.

The method of rapid cooling from the melt does not provide the same average cooling rate from one sample to another, and every sample must be carefully checked by x-ray diffraction. A

diffractometer equipped with a LiF curved crystal monochromator located in the diffracted beam was used for this purpose. Since the intensity of a beam diffracted by an amorphous specimen is relatively low, it cannot be reliably measured with a rate-meter, and either the fixed-count, or the fixed-time method must be used. The latter was chosen for this investigation. The diffractometer was driven at a speed of 0.02° (in 2θ) in 100 sec, and the total number of accumulated counts was printed on a tape every 400 sec, which corresponds to an angular interval of 0.08° in 2θ. The diffraction pattern was limited to the first "band" of the amorphous alloy which is between 2θ angles of 32° and 56°. About 34 hours were required to record a pattern. Under these conditions, the presence of a small amount of a crystalline phase imbedded in the amorphous matrix gives rise to relatively weak but quite distinct Bragg's peaks. Quenched foils which showed any deviation from a smooth amorphous diffraction band were rejected.

The progressive change from the amorphous to the crystalline state was followed by electrical resistivity and x-ray diffraction measurements. For the resistivity measurements the samples were heated at a constant rate of 1°C/minute. The x-ray study was carried out on samples heated for 20 minutes at constant temperature, with temperature increments of 20°C, so that the average rate of heating of these samples was also 1°C/min. The specimens used for resistivity measurements were rectangles about 22 x 5 mm. The standard four-points-probe method was used, with current and potential leads made of 0.005 in. Pt wires spot-welded to the specimen.

The effect of thermal gradients was minimized by current reversal. Because of the uncertainties in measuring the dimensions of such small specimens, the uncertainty in the absolute value of the resistivity is about 15%, and the results are given in terms of the ratio of the resistance of the specimen at a given temperature to that at room temperature. The uncertainties in relative resistivity values are about ± 0.2%. The specimens were placed in an evacuated fused silica tube and heated in a horizontal tube furnace. The temperature was measured by a Pt-PtRh thermocouple (0.005 in. diam) spot welded to the specimen and connected to a Leeds and Northrup K-5 potentiometer. The uncertainty in temperature measurements is probably less than ± 1°C.

The specimens used for following the crystallization by x-ray diffraction were rectangular foils about 10 x 15 mm. These specimens were large enough to cover the x-ray beam, having 1° divergence, in the angular range from 32° to 56° in 2θ. The isochronal annealing was performed in a helium atmosphere in a fused silica tube placed on a furnace with the temperature controlled within ± 1°C. The temperature range was from 20°C to 880°C, in steps of 20°C. The time it took for the specimen to reach temperature after immersion in the furnace was first determined on dummy specimens with a thermocouple spot-welded on them. This time was between 5 and 10 minutes, depending on the temperature, and this was taken into account, so that the time at the desired temperature was very close to 20 minutes for all temperatures. For these heat treatments, the foil was inserted into a holder (made of nickel) which could be

accurately relocated in the diffractometer after each isothermal treatment. This procedure was required because the amorphous foils become so brittle during crystallization that they cannot be safely handled, even with a pair of tweeezers.

After each isochronal anneal an x-ray diffraction pattern was recorded as previously described for the amorphous foils. As crystallization progressed, however, the angular range in 2θ between two successive recordings of counts was reduced from 0.08° to 0.04° and finally to 0.02°, in order to progressively increase the resolution of the diffraction pattern as the crystalline peaks became sharper.

Since the equilibrium diagram of ternary Fe-P-C alloys is not well known,[13] a few thermal analysis experiments were performed on the particular $Fe_{75}P_{15}C_{10}$ composition. The alloy was contained in a 12 mm fused quartz crucible maintained under argon atmosphere and the temperature was measured with a Pt-PtRh thermocouple protected by a fused silica tube immersed into the melt. The molten FePC alloy does not react with fused silica very rapidly and if the melt is not maintained above the liquid temperature more than about 10 to 20 min., no reaction with the crucible could be detected. The solid specimen was therefore inserted in the furnace at 950°C, and cooling was started as soon as possible after melting. The cooling curve was recorded at a cooling rate of about 5°C/min.

Thermal analysis was also performed on the amorphous alloy to record the temperature at which, if the heating rate is high enough, the amorphous to crystalline transformation takes place very rapidly

with a large heat release. As explained in Ref. 7, this temperature can be measured by spot welding a fine thermocouple made of 0.005 in. diam. Pt-PtRh wires to a small piece of foil about 3 to 5 mm square and 40-50μ thick.

II. III. RESULTS

A. Equilibrium Phases in $Fe_{75}P_{15}C_{10}$ Alloy

The phase boundaries in the ternary system FePC were first determined for the composition $Fe_{75}P_{15}C_{10}$. Cooling curves were obtained on four different specimens. Since these alloys have a pronounced tendency to undercool, the melt was seeded at frequent intervals. A liquidus temperature at 965°C followed by a well defined eutectic at 940°C were observed. This is probably a ternary eutectic between γ Fe saturated with P and C at that temperature, Fe_3P and Fe_3C. Another well defined arrest was present at 710°C and is most probably due to the transformation of γ Fe into α Fe plus Fe_3C, since the temperature is close to that corresponding to the same reaction in binary Fe-C alloys (723°C).

The structure of an alloy slowly cooled from the melt, and then kept for 2 weeks at 700°C was studied by microscopy and x-ray diffraction. The microstructure was typical of a cast alloy, with primary crystals of Fe and a fine eutectic structure of Fe_3P plus Fe_3C. The x-ray diffraction pattern of this alloy obtained with the diffractometer technique described in Section II.II. confirmed the presence of these three phases and the results are given in Table I. A few specimens were also quenched from 800 and 850°C, and as expected, a certain amount of retained austenite was detected by x-ray diffraction. In order to obtain the equilibrium structure of an amorphous alloy, a foil sealed in an evacuated quartz tube was rapidly heated to 850°C, maintained at that temperature for two weeks. The x-ray diffraction pattern of this foil was practically

TABLE I

RESULTS OF X-RAY DIFFRACTION PATTERNS OF SAMPLE HEATED AT 880°C FOR TWO WEEKS AND COOLED IN FURNACE

2θ (°)	Intensity (counts in 100 sec)	Interplanar Spacing d	(h k ℓ)	Phases
35.62	540	2.52	(301)	Fe_3P
40.90	3,750	2.20	(231)	Fe_3P
41.95	1,000	2.152	(330)	Fe_3P
42.70	2,100	2.116	(112)	Fe_3P
44.56	12,100	2.032	(110)	α - Fe
45.06	440	2.010	(103)	Fe_3C
45.68	2,750	1.984	(411)	Fe_3P
49.52	700	1.839	(222)	Fe_3P
51.00	660	1.789	(150)	Fe_3P
51.64	900	1.768	(312)	Fe_3P
54.26	400	1.689	(501)	Fe_3P
64.92	1,560	1.435	(200)	α - Fe
82.24	2,060	1.171	(211)	α - Fe

identical to that of a cast alloy subjected to the same heat treatment.

The intensity of the (110) reflection of Fe (Table I) is relatively high, but since this is a very strong reflection compared with all the reflections of Fe_3P and Fe_3C, it does not mean that the amount of the Fe phase in the equilibrium alloy is high. In fact, if P and C were insoluble in Fe, the alloy would not contain any Fe, since there is just enough Fe in $Fe_{75}P_{15}C_{10}$ to form 3 Fe_3P+2 Fe_3C. It is difficult to ascertain how much P and C are retained in the Fe phase. With only three reflections in the Fe pattern sharp enough for lattice parameter determination, the effect of carbon, which is small, and that of P, which according to Ref. 14 is not measurable, would be within the experimental uncertainties. Assuming that the solubilities of P and C in Fe are the same as those in the two binary systems at 700°C, (about 2 at.% for P and 0.2 at.% for C) the approximate composition of the equilibrium alloy would be 56 at.% Fe_3P, 37 at.% Fe_3C and 7 at.% Fe. The Fe content would be increased if the solubility limits in the ternary FePC system were increased at the particular composition $Fe_{75}P_{15}C_{10}$. The order of magnitude of the amount of Fe phase is not in contradiction with what can be estimated from the microstructure, namely anywhere between 5 and 10%.

B. Crystalline Phases present after a Sudden Heat Release at High Rates of Heating

At heating rates of about 300°C/sec and above, a sudden heat release was observed around 430°C. This temperature is not exactly reproducible from specimen to specimen, but the scatter is less than about ±10°C. In order to study the structure of a specimen imme-

diately after the heat release, the specimen was rapidly removed from the furnace as soon as the rise in temperature took place. A typical temperature-time diagram for this case is shown by curve 1 in Fig. 1. The sudden rise in temperature corresponds to a heat release of about 900 kcal/mole.[7] At lower rates of heating, about 100°C/sec, two heat releases were observed. The first one occurs also at 420°C and was relatively small, and this was immediately followed by a large heat release. The temperature interval between the two heat releases is probably less than 5°C. To study the structure of a specimen after the small heat release, a specimen was heated at a rate of about 100°C/sec and taken out of the furnace after the small temperature increase, as shown by curve 2 in Fig. 1. The phases present in these specimens were identified by x-ray diffraction and electron diffraction and the results are presented in Tables II and III. After the small heat release (rate of heating of 100°C/min) only three very broad diffraction peaks were present in the x-ray diffraction pattern and were attributed to the presence of γ Fe, Fe_2P and Fe_3P. Electron diffraction confirmed the presence of γ Fe, and Fe_2P. After the large heat release, the x-ray diffraction peaks were relatively sharper and more intense but the accuracy in measuring d spacings was still limited to two decimals as shown in Table II. The phases were identified as α Fe, Fe_3P and Fe_3C. One diffraction ring in the electron diffraction pattern corresponded to the (331) reflection of Fe_3C, but this may not constitute enough evidence to definitely establish the presence of this phase. Electronmicrographs were taken after the large heat release (Fig. 2a) and after the small heat

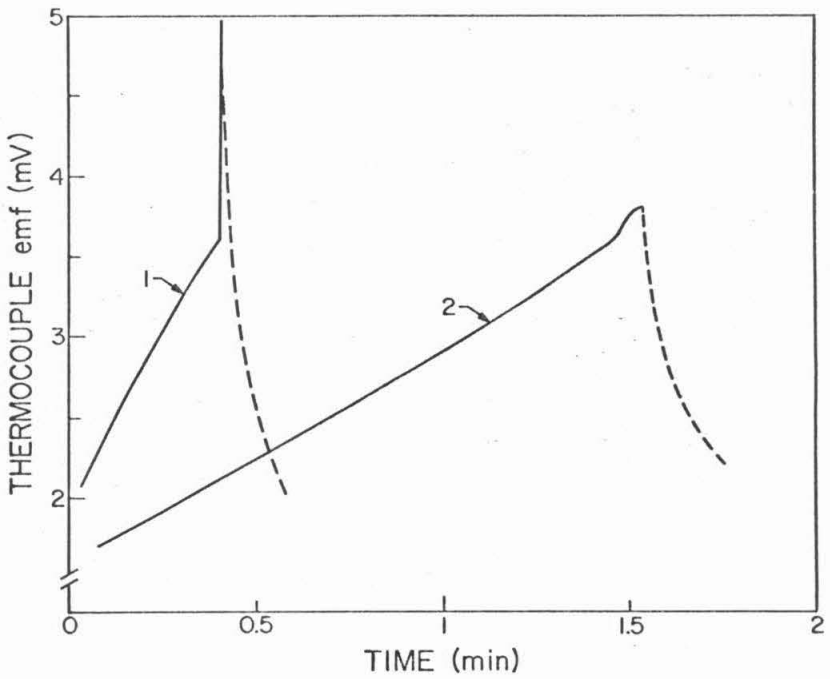

Fig. 1. Temperature vs. time curve of amorphous alloy heated at a rate of 320°C/min (curve 1) and 100°C/min (curve 2).

TABLE II

RESULTS OF X-RAY DIFFRACTION PATTERN OF SAMPLES USED FOR THERMAL ANALYSIS

2θ (°)	Intensity (counts in 100 sec)	Interplanar Spacing d (Å)	(h k ℓ)	Phases
Heated up to 435°C at a rate of 320°C/min				
35.90	100	2.50	(301)	Fe_3P
37.80	50	2.38	(112)	Fe_3C
41.22	2,300	2.19	(231)	Fe_3P
42.42	400	2.13	(330)	Fe_3P
42.86	2,000	2.11	(112)	Fe_3P
44.68	7,000	2.03	(110)	α - Fe
46.02	1,400	1.97	(411)	Fe_3P
49.74	600	1.83	(222)	Fe_3P
51.84	900	1.76	(312)	Fe_3P
Heated up to 435°C at a rate of 100°C/min				
35.28	610	2.54	(200	Fe_2P
43.70	2,250	2.07	(111)	γ - Fe
50.19	100	1.79	(150)	Fe_3P

TABLE III

RESULTS OF ELECTRON DIFFRACTION PATTERNS OF SAMPLES USED FOR THERMAL ANALYSIS

Radius of Rings (cm)	Interplanar Spacing d (Å)	(h k ℓ)	Phases
Heated up to 435°C at a rate of 320°C/min			
0.85	2.22	(002)	Fe_3P
0.94	2.01	(110)	α - Fe
0.03	1.83	(222)	Fe_3P
1.30	1.45	(200)	α- Fe
1.44	1.31	(442)	Fe_3P
1.70	1.11	(331)	Fe_3C
1.90	0.99	(220)	α - Fe
2.25	0.84	(222)	α - Fe
Heated up to 435°C at a rate of 100°C/min			
0.92	2.08	(111)	γ - Fe
1.58	1.21	(401)	Fe_2P

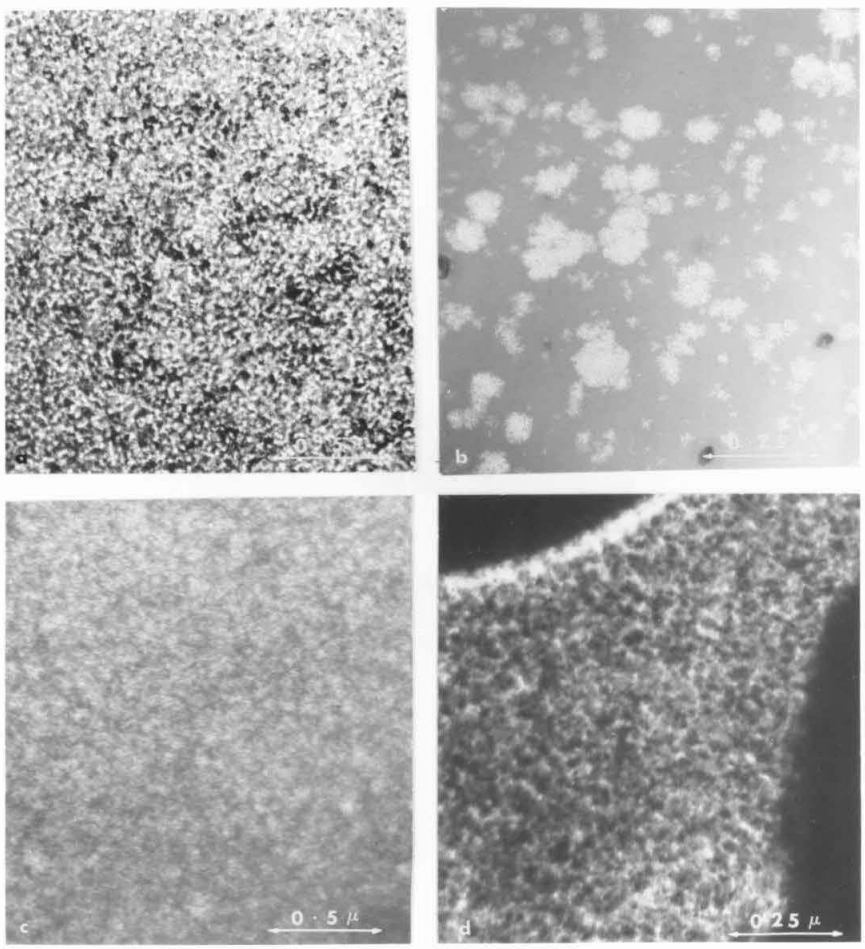

Fig. 2. Electronmicrographs of amorphous FePC alloys: (a) after the large heat release at a heating rate of 320°C/min.; (b) after the small heat release at a heating rate of 100°C/min; (c) after heating at a rate of 1°/min up to 375°C; (d)after heating at a rate of 1°/min up to 880°C.

release (Fig. 2b). After the large heat release the structure appears to be entirely microcrystalline with an average crystal size estimated to be less than about 300 Å. After the small heat release, the bulk of the specimen was still amorphous, and this is confirmed by the presence of a broad amorphous diffraction band in the x-ray diffraction pattern. Isolated clusters of microcrystalline phases could be seen in electronmicroscopy and their size ranges from 100 Å to about 2, 000 Å.

The results of these experiments show that the crystallization of the amorphous $Fe_{75}P_{15}C_{10}$ alloy is greatly influenced by the rate of heating. At high enough rates (above about 320°C/min), the crystalline phases nucleate and grow very fast with a large heat release, and these phases are the equilibrium phases. At lower rate, it is possible to stop the growth of crystalline phases, and this results in a transient structure made of the amorphous matrix and isolated clusters containing metastable phases (γ Fe + Fe_2P).

C. Progressive Crystallization at a Rate of Heating of 1°C/min.

The transformation from the amorphous to the crystalline state was followed by both electrical resistivity measurements and x-ray diffraction. A typical curve of resistivity vs. temperature taken at a rate of heating of 1°C/min is shown in Fig. 3. The resistivity increases linearly (slope of 10^{-3}/°C) up to about 310°C. Although a small anomaly in resistivity seems to occur around 320°C on the graph of Fig. 3, a plot with an expanded vertical scale shown in Fig. 4, indicates a definite break in the resistivity curve at 325°C. This change of slope of the resistivity temperature curve is due to

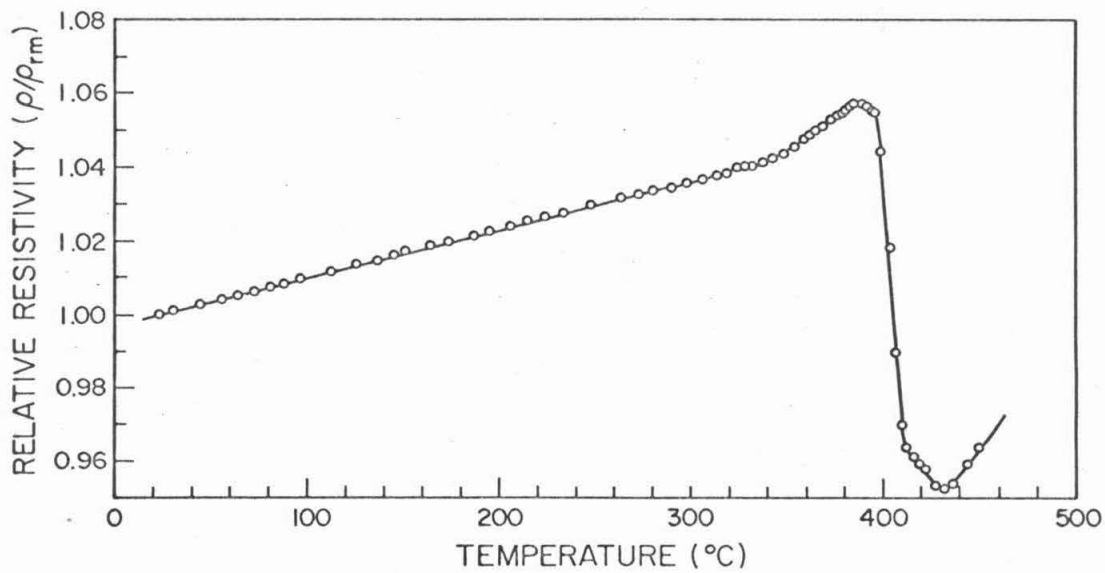

Fig. 3. Relative resistivity vs. temperature of amorphous FePC alloy heated at a rate of 1°C/min.

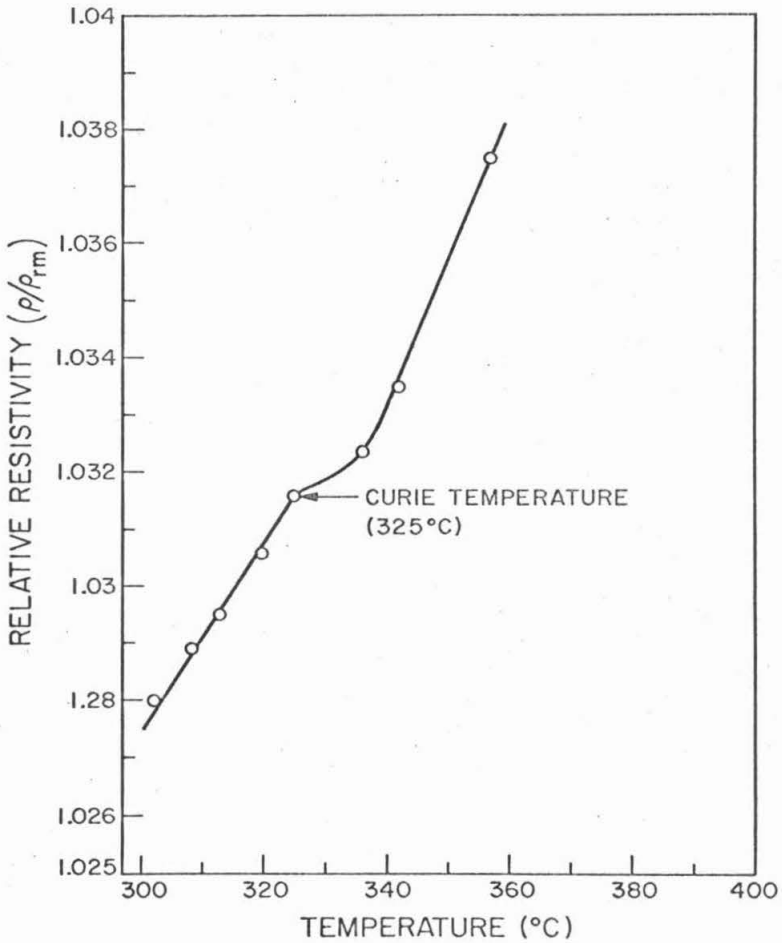

Fig. 4. Curie Temperature of Amorphous FePC from resistivity vs. Temperature Curve

the ferromagnetic to paramagnetic transition which has been reported to be about 320°C.[15]

Above 310°C, the slope of the resistivity curve increases slowly and the resistivity goes through a maximum at about 390°C then drops very sharply and starts increasing again above 430°C. This drop was previously observed in other amorphous alloys and is due to the rapid transformation from the amorphous to the crystalline state.[4, 16] The increase in the slope of the resistivity-temperature curve before the onset of massive crystallization has been observed in a number of amorphous alloys[17, 18] but no satisfactory explanation has been given as to its origin. In order to gain more information, experiments were performed in which the temperature was increased up to a point located on the upward branch of the resistivity curve, and then decreased. The results of these measurements are shown in Fig. 5 and the conclusion is that the additional increase in resistivity above the linear increase is not a reversible phenomenon and might be the result of structural changes in the amorphous alloy. A specimen was then heated at the rate of 1°C/min up to 375°C and its structure was investigated by electronmicroscopy. As shown in Fig. 2c, the presence of a microcrystalline phase dispersed in the amorphous matrix was detected. Although this phase could not be well resolved, the average crystallite size can be estimated to be about 50 Å. Electron diffraction patterns obtained from this specimen were analyzed and as shown in Table IV, the diffraction rings could be indexed as those of an Fe_2P phase, which is not an equilibrium phase in the $Fe_{75}P_{15}C_{10}$ alloy.

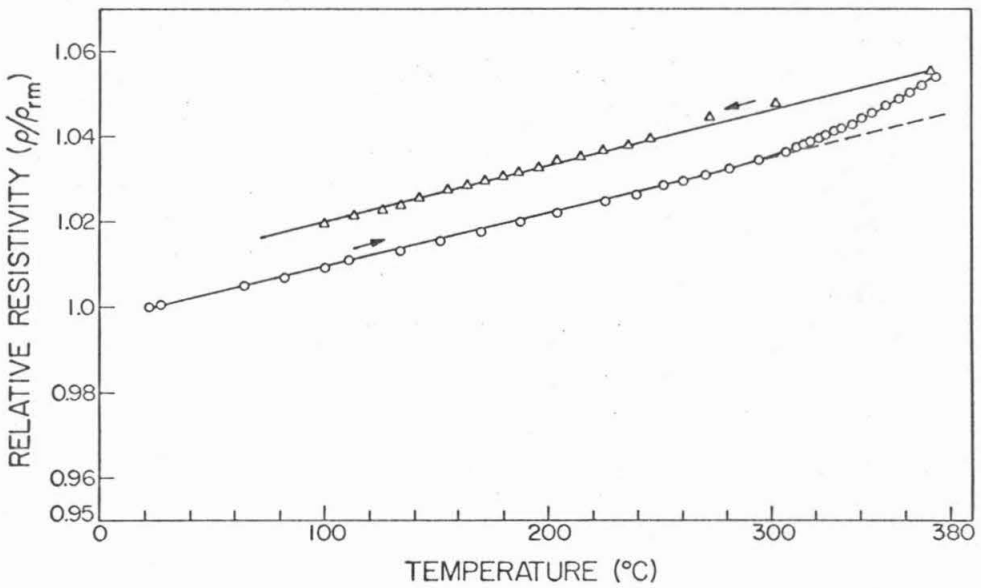

Fig. 5. Relative resistivity vs. temperature curve showing the non-reversibility of the resistivity increase above 310°C

TABLE IV

RESULTS OF ELECTRON DIFFRACTION PATTERN OF SAMPLE HEATED UP TO 375°C AT A RATE OF 1°C/MIN

Radius of Rings R (cms)	Interplanar Spacing d (Å)	(h k ℓ)	Phases
0.94	2.05	(200)	Fe_2P
1.60	1.20	(401)	Fe_2P
1.87	1.03	(213)	Fe_2P

The presence of a dispersed microcrystalline phase in the range of 310°C to 390°C may explain the increase in resistivity, if it is assumed that very small crystalline clusters imbedded in an amorphous matrix are analogous to microcrystalline precipitates in a crystalline matrix. According to Mott[19] the increase in electrical resistivity observed during the formation of Guinier-Preston zones in the early stage of precipitation in an age-hardenable alloy, is due to the scattering of conduction electrons by the precipitate particles. The critical radius of G-P zones for resonant scattering is close to the wave length of the conduction electron. Using a modified model[20] the value of the critical radius for the $Fe_{75}P_{15}C_{10}$ alloy is estimated to be about 30 Å, which is of the order of magnitude of the average size of crystalline clusters in FePC deduced from electronmicroscopy observation (about 50 Å).

As described in Section II, x-ray diffraction patterns were obtained on specimens heated for 20 minutes at constant temperatures in increments of 20°C, corresponding to an average rate of heating of 1°C/min. Measurements were taken within an angular range which includes the first broad diffraction band of the amorphous structure (from 32° to 56° in 2θ angles). This range includes only one reflection for α iron, namely the (110), nine reflections for Fe_3P and one reflection for Fe_3C. During the isochronal anneal, the diffraction pattern of the amorphous alloy did not show any detectable change up to 400°C. The maximum intensity at the peak of the band (at 43.85° in 2θ) and its half width (about 5.50 in 2θ) remain constant. From 400 to about 800°C, the peak intensity of the

amorphous band decreased as indicated in Fig. 6. The first detectable crystalline peak was the (110) reflection of α Fe, at 380°C. Between 400 and 420°C, two peaks of Fe_3P (231) and (112) became noticeable. The increase in the intensities of these three peaks with increasing temperature are shown in Fig. 7. Between 420 and 440°C there is a very marked sudden increase in intensity, which shows that within this range, crystallization has progressed very rapidly. This result is in agreement with the observed sudden heat release observed in specimens heated at rates above about 300°C/min. The rapid drop in electrical resistivity attributed to the disappearance of the amorphous phase occurred between about 390 and 410°C. This temperature interval is therefore about 30°C lower than that deduced from x-ray diffraction measurements. The lack of correspondence between the two types of measurements may be due to two reasons. First, the electrical measurements were performed continuously while the specimen was heated at a rate of 1°/min, whereas the x-ray measurements were obtained by isochronal annealing by steps of 20°C, and the cooling of the specimen back to room temperature after every step may have a retarding action on the progress of crystallization. Second, the time it took to bring the specimen up to the desired temperature in the isochronal annealing experiments may have been underestimated, so that the actual time at temperature was probably less than 20 minutes. It is therefore believed that the difference between the two kinds of measurements is due to experimental uncertainties, and the discontinuity in x-ray peak intensities and the sudden drop in resistivity correspond to the rapid progress of

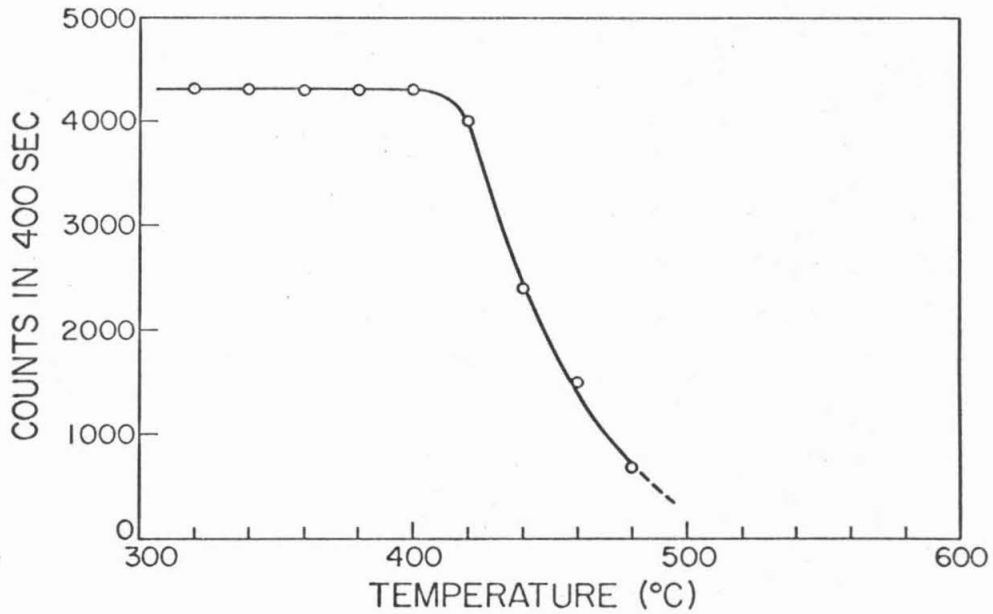

Fig. 6. Intensity of the peak of the amorphous diffraction band vs. temperature (average rate of heating 1°C/min)

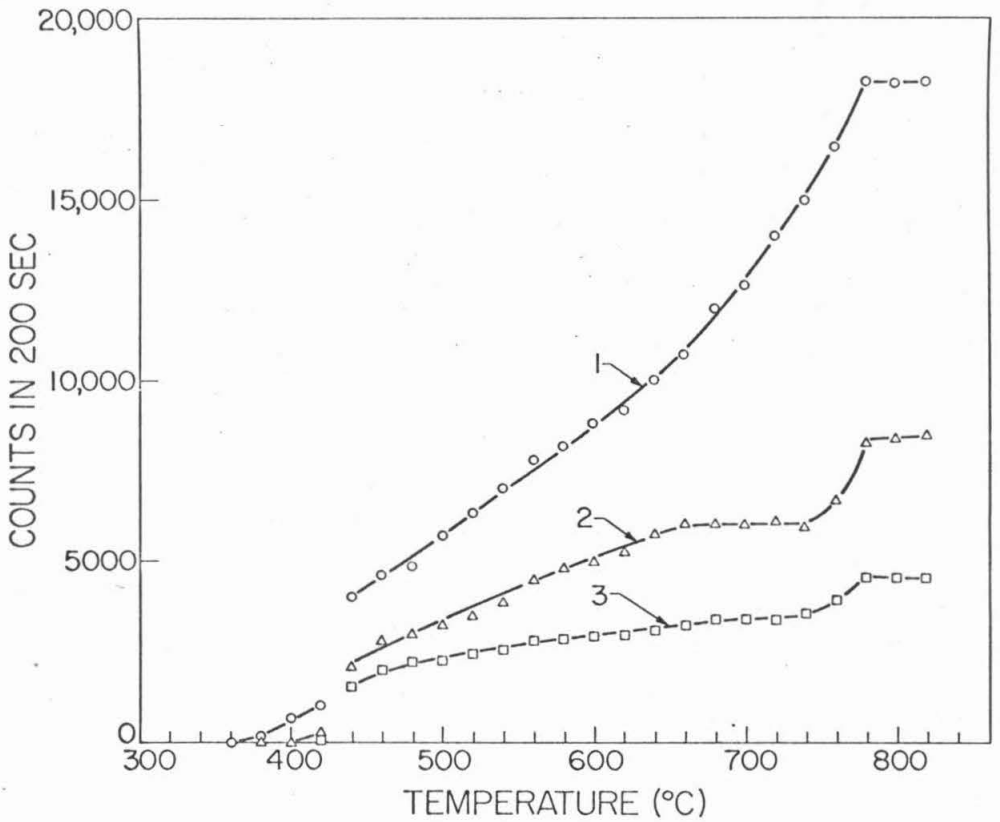

Fig. 7. Peak intensity of x-ray reflections vs. temperature; Curve 1, (110) of α Fe; Curve 2, (231) of Fe_3P; Curve 3, (112) of Fe_3P.

crystallization.

The resistivity-temperature curve shown in Fig. 3 is limited to about 450° C. The results of measurements above this temperature were unreliable, because visible cracks were present in all specimens investigated. As soon as the specimen becomes microcrystalline, it is so brittle that the change in volume associated with the amorphous to crystalline transformation (of the order of 2 to 5%) creates high enough stresses to produce local rupture of the specimen.

As shown in Fig. 7, the peak intensity of the (110) line of Fe increases steadily up to about 780° C. This increase may be due to an increase in the amount of the Fe phase or to a growth in crystallites size. Since the amorphous phase seems to have practically disappeared around 500°C (see Fig. 6) the increase in the size of the crystallites is probably the main reason for the increase in peak intensity which is due to a progressive sharpening of the diffraction lines. Measurements of the crystallite size at the end of the isochronal annealing (880° C) confirm this explanation. An electron-micrograph of the crystallized sample obtained by heating at a rate of 1° C/min up to 880°C, and shown in Fig. 2d, revealed that the average grain size at 880° C was about 400 Å, and hence the grain size increased from about 50 Å at 375° to about 400 Å at 880°C. In this range, appreciable broadening should be present, and should decrease with increasing temperature, resulting in a progressive increase in peak intensity, as shown in Fig. 7. A better correlation between the intensity of the (110) reflection and the amount of α Fe

phase present could have been obtained by measuring the integrated intensity of the reflection, but this procedure proved to be difficult because of the overlapping of reflections due to Fe_3P.

The peak intensity of the two strong reflections of the Fe_3P phase as a function of temperature shown in Fig. 7, has the same general shape as that of the (110) reflection of α Fe. A sudden increase occurs in the temperature range of 420 to 440°C corresponding to the onset of crystallinization. Instead of a continuous increase up to 780°C, the peak intensities of the Fe_3P reflections seem to have a plateau starting around 660°C, followed by a sharp increase around 740°C. No intensity increase takes place above 780°C, which is exactly the temperature at which the intensity of the (110) reflection of α Fe ceases to increase. These changes in the rate of growth of the crystallites of the various phases may be connected with the temperatures of phase boundaries in the ternary Fe-P-C system. Since the equilibrium diagram of this system is not known, such a correlation cannot be quantitatively substantiated. In addition it should be pointed out that isochronal experiments do not correspond to equilibrium conditions, and this adds to the difficulty in interpreting the results.

In principle, the curves shown in Fig. 7 could have been extended to a temperature corresponding to the eutectic melting point of the $Fe_{75}P_{15}C_{10}$ alloy (940°C). This was found to be impossible, because above about 820°C, the amorphous foils heated at a rate of 1°C/min fell into pieces. A given area of the specimens could not be replaced in the diffractometer in exactly the same position, and

intensity measurements became meaningless. Rapid heating of an amorphous foil by immersion of a specimen in a furnace at 880°C, however, retained the integrity of the foil, and after two weeks at temperature, the intensity of the (110) of α Fe was about 1.4 times larger than that shown in Fig. 7. This result indicates that equilibrium conditions were not reached after heating at the rate of 1°/min up to 820°C and may not even have been reached after 2 weeks at 880°C temperature. Obviously isochronal annealing cannot lead to a clear understanding of the kinetics of transformation from the amorphous to the crystalline state, and isothermal annealing should be used. Unfortunately, this would lead to an unmanageable number of experiments to be conducted with furnaces maintained at constant temperatures for a period of one to ten years. The results of the isochronal annealing reported here bring in focus the complexity of the amorphous to crystalline transformation in FePC alloys.

II. IV. CONCLUSIONS

The rate and the mode of crystallization of an amorphous $Fe_{75}P_{15}C_{10}$ alloy obtained by rapid cooling from the liquid state have been studied by thermal analysis, x-ray diffraction, electron-microscopy and electrical resistivity. The results of this investigation show that the rate, as well as the morphology of the amorphous to crystalline transformation greatly depend on the rate of heating. At very high rates of heating (above about 300°C/min) the transformation is very rapid and is accompanied by a large heat release of the order of 900 cal/mole. The phases present after the heat release seem to correspond to the equilibrium ones, namely α Fe saturated in P and C, Fe_3P and Fe_3C. At lower rates of heating, it is possible to stop the crystallization process so that the specimen consists of clusters of microcrystals imbedded in an amorphous matrix. Under these conditions, the crystalline clusters contained the Fe_2P phase, which subsequently disappears at higher temperature. The results of experiments performed at a relatively small rate of heating of 1°C/min confirm the more or less discontinuous nature of the process of nucleation and growth of the equilibrium phases, as evidenced by the sudden increase in the peak intensity of the Fe and Fe_3P x-ray diffraction peaks around 430°C, which is near the temperature at which sudden crystallization occurs at high rates of heating. A better understanding of the early stages of crystallization could be gained by making isothermal aging experiments within the critical temperature range between 340 and 460°C and studying the progress of crystallization over very long periods of time.

The crystallization of amorphous FePC is accompanied by a very sharp drop in electrical resistivity. About 60° C before this drop occurs, the resistivity increases faster than linearly with temperature. This behavior has been observed in a number of amorphous alloys and several explanations have been proposed. It was found in the present case that the increase in resistivity, in this temperature range is not reversible. Electronmicroscopy observations show that in this temperature range clusters of microcrystalline phases are imbedded in the amorphous matrix. It is suggested that these microcrystalline precipitates act as scattering centers for the conduction electrons, in a manner similar to that found in the early stage of precipitation (Guinier-Preston zones) in supersaturated crystalline solid solutions.

REFERENCES

1. S. Mader, J. Vacuum Science and Techn., 2, 35, (1965).
2. Pol Duwez, Progress in Solid State Chemistry, Vol. 3, p. 377, Pergamon Press, Oxford and New York (1966).
3. W. Klement, Jr., R. H. Willens and Pol Duwez, Nature 187, 809, (1960).
4. Pol Duwez, R. H. Willens and R. C. Crewdson, J. Appl. Phys. 36, 2267, (1965).
5. H. L. Luo and Pol Duwez, Appl. Phys. Letters, 2, 21, (1963).
6. H. L. Luo, Ph. D. Thesis, California Institute of Technology, (1964).
7. Pol Duwez and S. C. H. Lin, J. Appl. Phys., 38, 4096, (1967).
8. S. C. H. Lin and Pol Duwez, Phys. Stat. Sol., 34, 469, (1969).
9. S. C. H. Lin, J. Appl. Phys., 40, 2173, (1969).
10. S. C. H. Lin, J. Appl. Phys., 40, 2175, (1969).
11. P. Pietrokowsky, Rev. Sci. Instr., 34, 445, (1962).
12. D. R. Harbur, J. W. Anderson, and W. J. Maraman, Trans. A.I.M.E., 245, 1055, (1969).
13. C. H. Desch, Correspondence to Stead's Paper, J. Iron Steel Inst., 91, 195, (1915).
14. G. Hägg, Z. Krist, 68, 470, (1958).
15. C. C. Tsuei, G. Longworth and S. C. H. Lin, Phys. Rev. 170, 603, (1968)
16. S. Mader, H. Widmer, F. M. d'Heurle and A. S. Nowick, Appl. Phys. Letters, 3, 201, (1963).

REFERENCES (Cont'd)

17. H. S. Chen and D. Turnbull, J. Chem. Phys., 48, 2560, (1968).

18. P. L. Maitrepierre, J. Appl. Phys., (Accepted for Publication).

19. N. F. Mott, J. Inst. Metals, 60, 267, (1937).

20. R. Labusch, Phys. Stat. Sol., 3, 1661, (1963).